AFGL-TR-89-0031

Feasibility of Millimeter-Accuracy Geodetic Positioning and Vehicle Tracking With Repeater Satellites

Laureano Alberto Cangahuala

Massachusetts Institute of Technology
77 Massachusetts Avenue
Cambridge, MA 02139

27 January 1989

Scientific Report No. 2

AIR FORCE GEOPHYSICS LABORATORY
AIR FORCE SYSTEMS COMMAND
UNITED STATES AIR FORCE
HANSCOM AIR FORCE BASE, MASSACHUSETTS 01731-5000

UNCLASSIFIED
SECURITY CLASSIFICATION OF THIS PAGE

REPORT DOCUMENTATION PAGE

1a. REPORT SECURITY CLASSIFICATION: UNCLASSIFIED	1b. RESTRICTIVE MARKINGS: N/A
2a. SECURITY CLASSIFICATION AUTHORITY	3. DISTRIBUTION / AVAILABILITY OF REPORT: Approved for public release; distribution unlimited.
2b. DECLASSIFICATION / DOWNGRADING SCHEDULE	
4. PERFORMING ORGANIZATION REPORT NUMBER(S)	5. MONITORING ORGANIZATION REPORT NUMBER(S): AFGL-TR-89-0031
6a. NAME OF PERFORMING ORGANIZATION: Massachusetts Institute of Technology; 6b. OFFICE SYMBOL (If applicable): Room 37-552	7a. NAME OF MONITORING ORGANIZATION: Air Force Geophysics Laboratory
6c. ADDRESS (City, State, and ZIP Code): 77 Massachusetts Avenue Cambridge, MA 02139	7b. ADDRESS (City, State, and ZIP Code): Hanscom Air Force Base, MA 01731-5000
8a. NAME OF FUNDING / SPONSORING ORGANIZATION: Air Force Geophysics Laboratory; 8b. OFFICE SYMBOL (If applicable): AFGL/LWG	9. PROCUREMENT INSTRUMENT IDENTIFICATION NUMBER: F19628-86-K-0009
8c. ADDRESS (City, State, and ZIP Code): Hanscom Air Force Base, MA 01731-5000	10. SOURCE OF FUNDING NUMBERS: PROGRAM ELEMENT NO. 61102F; PROJECT NO. 2309; TASK NO. G1; WORK UNIT ACCESSION NO. BN

11. TITLE (Include Security Classification)
FEASIBILITY OF MILLIMETER-ACCURACY GEODETIC POSITIONING AND VEHICLE TRACKING WITH REPEATER SATELLITES

12. PERSONAL AUTHOR(S): Cangahuala, Laureano Alberto

13a. TYPE OF REPORT	13b. TIME COVERED	14. DATE OF REPORT (Year, Month, Day)	15. PAGE COUNT
Scientific No. 2	FROM 86Apr29 TO 89Jan27	89 Jan 27	78

16. SUPPLEMENTARY NOTATION
Student thesis submitted to the Dept. of Aeronautical and Astronautical Engineering in partial fulfillment of Master of Science degree requirements at Mass. Inst. of Technology

17. COSATI CODES		
FIELD	GROUP	SUB-GROUP
08	05	--

18. SUBJECT TERMS (Continue on reverse if necessary and identify by block number)
Satellite geodesy, satellite positioning, satellite communications, repeater satellites, space geodesy, radio positioning, radio interferometry, radio tracking

19. ABSTRACT (Continue on reverse if necessary and identify by block number)

The feasibility of the GeoBeacon system proposed by Prof. Counselman of M.I.T. is studied. In this system, low-power radio transmitters are placed on vehicles or at other points whose positions are to be monitored. Tropospheric and ionospheric refraction are also monitored. The number of transmitters is practically unlimited. Signals from all transmitters in view are repeated by satellites to a central site where detection, measurement, and data processing take place. To enable precise geodetic positioning, signals would be emitted at multiple frequencies, including relatively low (*e.g.* 100 MHz) and relatively high (several GHz) frequencies. The lower frequency signals would aid the acquisition and tracking of the higher frequency signals in order to reduce transmitter-power requirements. Power requirements are calculated as functions of frequency from 100 MHz to 50 GHz, considering both natural phenomena and interference from accidental and intentional radio transmissions. An algorithm is developed for the selection of frequencies by which aided tracking of the highest frequency signal can be maintained. This algorithm is based on a stochastic description of the kinematic and ionospheric contributions to the received signal frequencies and phases. Discrete Kalman filter equations are derived for estimating the covariances of phase and frequency estimates.

20. DISTRIBUTION / AVAILABILITY OF ABSTRACT	21. ABSTRACT SECURITY CLASSIFICATION
☐ UNCLASSIFIED/UNLIMITED ☒ SAME AS RPT. ☐ DTIC USERS	UNCLASSIFIED

22a. NAME OF RESPONSIBLE INDIVIDUAL	22b. TELEPHONE (Include Area Code)	22c. OFFICE SYMBOL
Dr. Thomas P. Rooney	(617) 377-3486	AFGL/LWG

DD FORM 1473, 84 MAR — 83 APR edition may be used until exhausted. All other editions are obsolete.

SECURITY CLASSIFICATION OF THIS PAGE
UNCLASSIFIED

Table of Contents

Figures and Tables

1. Introduction

The tool that has most advanced man's positioning capability is the satellite. By positioning we refer to a broad range of applications that satellite positioning systems have made more accurate and reliable. For instance, positioning includes traditional construction surveying (e.g., for buildings, highways) as well as the development of large scale geodetic networks for boundary determination, aerial radar mapping, and gravity field measurements. Detection of local position changes (e.g., mining subsidence, structural deformation) and of changes more global in scale (e.g., plate tectonics, volcano growth) can also be monitored by satellite positioning systems. Also, since line-of-sight contact is not needed between sites, satellite positioning can aid in monitoring the location of large fleets of taxi cabs, trucks and railcars.[1]

In general, the introduction of satellites to geodesy has brought with it many advantages over traditional land surveying techniques. First, since visual contact is not needed between baseline ends in satellite geodesy, the allowable area of investigation is virtually unlimited over the Earth's surface. Not only does the coverage area increase, but the number of man-hours needed per unit baseline distance is less than that required with line-of-sight surveying. Also, satellite receivers can be left at remote locations, whereas measuring these same sites with conventional methods requires the physical and computational effort of repeated visits to many sites for measurements. Finally, with worldwide coverage available through one system, all recorded locations can be tied to one global coordinate frame and one data base, thereby eliminating the difficulties involved in relating results from independent surveying campaigns.

Besides geodesy, positioning also includes navigation applications. For aircraft, ships, and spacecraft, this can include *en route* navigation, inertial navigation system

---

[1]Wells, Guide to GPS Positioning, Chapter 2.

updating, and precision maneuvers and approaches. Recreational users of satellite positioning systems can include pleasure boaters, mountain climbers, and eventually, auto drivers navigating through unfamiliar roads. Spacecraft in low earth orbit can use other positioning satellites for docking, radar imaging, or remote sensing. Positioning systems can also aid any these forms of transportation by serving as an emergency distress beacon.[1]

In addition to the possibilities of positioning systems mentioned, military applications include the acquisition and tracking of targets and remotely operated vehicles, as well as guidance, command, and control of missiles.

1.1. Overview of Extraterrestrial Positioning Systems

Before the existence of artificial satellites, extraterrestrial positioning techniques consisted of conventional astronomical positioning with a theodolite or sextant. The first satellite positioning systems were primarily used to improve the knowledge of the Earth's shape as well as the satellite's orbit parameters. This was accomplished by measuring the Doppler shift of the satellite's beacon. These early experiments evolved into the TRANSIT system, which began operation in 1961. In this positioning scenario, the user receives orbit information from messages transmitted by 6 satellites in 1100 km circular polar orbits. The user can compute his position by integrating the measured frequency shifts and using the transmitted orbit data.[2]

A second satellite system which operated on measured Doppler shifts began in 1978. Argos was a cooperative project among the French Centre National d'Etudes Spatiales (CNES), NASA, and the U.S. National Oceanic and Atmospheric Association (NOAA). The Argos user transmitted a signal at 401.65 MHz, which was received by a

---

[1] Ibid.

[2] Suggested further reading on the TRANSIT system: Stansell, T.A., The TRANSIT Navigation Satellite System, Magnavox Government and Industrial Electronic Company, Torrence, CA, 1978.

TIROS/N - class weather satellite, which then repeated the signal back to one of three tracking stations. All received signals were relayed to a central data processing center in Toulouse, France. Afterwards, the processed position and velocity results were mailed to the user. Accuracies of 3 km (3 σ) and 0.5 ms^{-1} (3 σ) were claimed in position and velocity, respectively. The system could handle up to 4000 transmitters simultaneously, assuming an even distribution of sites over the Earth's surface.

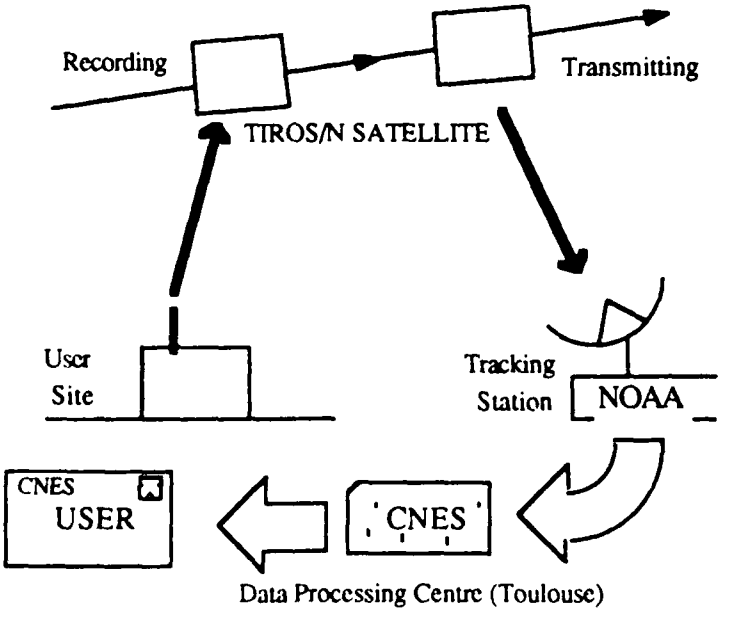

Figure 1. ARGOS Satellite System[1]

Another system that operates in a manner similar to Argos is the COSPAS-SARSAT search and rescue (SAR) system, a venture involving Canada, France, the United States and the Soviet Union. So far, the program has been responsible for saving over 1150 lives as of the fall of 1988. The success of COSPAS-SARSAT has led the federal government to require that all boats carry a SARSAT emergency transmitter by 1989. These transmitters operate at civil and military distress frequency allocations (121.5 MHz,

[1]Based on a viewgraph prepared by Canadian GPS Associates.

243 MHz), and their signals are eventually picked up by one of 5 satellites in the COSPAS-SARSAT system. The transmitter, sending a 0.5 s signal every 50 s, runs on a peak power of less than 100 mw, and costs as little as $150 in 1988.[1]

Currently, the most widely used satellite positioning system is the NAVSTAR (NAVigation Satellite Time And Ranging) Global Positioning System, hereafter referred to as GPS. When fully deployed in the mid- to late-1990's, the GPS will consist of: 18 (7 as of late 1988) satellites in 12-sidereal hour circular orbits; a ground-based control system to synchronize the satellites, update their broadcast messages, and monitor their health and orbits; and user receivers, which will acquire and track the signals from GPS satellites in view. A GPS receiver can distinguish between different satellites by either the coded modulation of the signal from each satellite or by having prior estimates of the satellite orbits and the Doppler shifts of the received signals. Position can be determined by measuring the group delay of the modulation and/or the phase delay of the carrier.

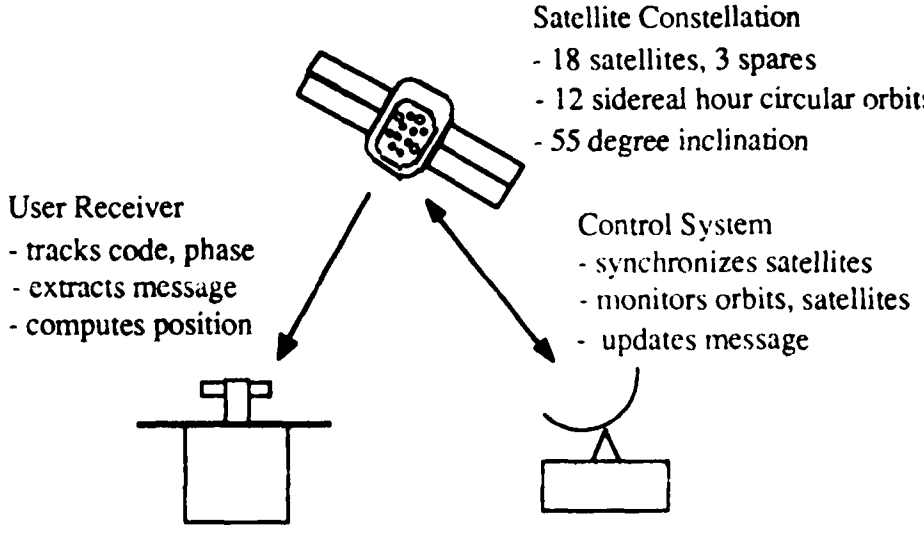

Figure 2. NAVSTAR Global Positioning System (GPS)

[1]Based on an emergency locator transmitter advertisement for Guns and Ammo magazine, mid-1988.

Positioning systems of the future include Geostar, a two-way positioning system with a demonstrated position accuracy of 1 meter and potential user terminal cost of $450.[1] Other systems that have been specifically designed to test orbit determination and geodetic techniques are planned or scheduled for deployment in the late 1990's. They include DORIS (Doppler Orbitography and Radio Positioning Integrated by Satellite), PRARE (Precise Range and Range Rate Equipment), and GLRS (Geodynamics Laser Ranging System).[2]

1.2. Capabilities and Limitations of GPS

Of all the positioning systems in use or in active development, GPS in principle holds the most promise for the wide range range of needs of the scientific and commercial communities. For example, through advances in signal processing and in obtaining accurate satellite ephemerides, GPS has made possible relative measurements over distances of the order or 2000 km with an accuracy on the order of 1 cm. By using quasar signals instead of satellite signals, the movements of the Earth's crustal plates in the western United States have already been accurately mapped;[3] these measurements are being repeated and extended with GPS. GPS can also be used to monitor the structural dynamics of dams, offshore oil drilling platforms, or the ground over areas of mining or water or oil removal.

Although poor satellite geometry may cause the fully operational GPS to suffer periodic degradation of performance, its accuracy already exceeds that of any naval navigation system in operation today. With the accuracy of the GPS and the reliability of

---

[1]Wells, Chapter 3.
[2]Herring, personal communication.
[3]Jordan and Minster, "Measuring Crustal Deformation in the American West," pp.48-58.

the terrestrial LORAN system, a Hybrid GPS/Loran system could become a powerful aviation navigation tool.[1]

In applications where position and velocity measurements are needed at many sites, however, using GPS brings up a problem of cost. In many of these applications, a project's success depends on how many locations (or objects) can be located and tracked at once. Except in studies where measurement sites are less than about 100 m apart, (e.g., in dam deformation), every location will require its own GPS receiver. Although the market prices of receivers should drop as the remaining GPS satellites are placed into orbit, the price of a receiver alone is currently on the order of $50,000 (1988 dollars). At these prices, these receivers can not be left unattended at sites where vandalism would be a problem. These costs make it prohibitive for any institution to perform measurements at more than tens of locations, or hundreds if the manpower needed to move dozens of receivers from point to point is available.

In any case, the required follow-up work for each campaign gives rise to a second problem. Specifically, there must also be a means for the data generated in all the receivers to be brought together. This would require additional visits to each receiver or the addition of another system to transmit the receiver data to a central processing site. A third problem is that the high power demands of geodetic receivers (at 20-200 w apiece) make it cumbersome for them to be self-powered by solar cells.

1.3. Motivation for a New Satellite Positioning and Tracking System

One method of circumventing the problems outlined above has been suggested by Prof. Charles Counselman. Small radio beacons each transmitting several frequencies are set up at the survey points, and a constellation of repeater satellites receive the signals (see

[1] van Graas, "Sole Means Navigation Through Hybrid Loran-C and GPS," pp. 147-160.

Figure 3 for an overview of the system, nicknamed "GeoBeacon").[1] All the received signals are then relayed to a central site where the processing is done for the entire network of transmitter sites. The first advantage of this scheme over the GPS positioning methodology, is that transmitters are cheaper than GPS receivers. These transmitters could be sold for relatively low prices, as are the SARSAT emergency beacons for outdoorsmen that were mentioned earlier. The GeoBeacon transmitter would need only a crystal oscillator to achieve the necessary frequency stability, and a means for "tagging" each transmitter's carrier signal with coded modulation. If the required uplink transmitter power were set low enough, these transmitters could be powered by solar cells and left at their respective sites without any return visits or maintenance checks. The second advantage of the system is that if a particular transmitter's signal (identified by its code) should no longer be received by the satellites, it can be replaced more cheaply than any GPS receiver could. This combination of 'throwaway' transmitter, brought by its lower cost, and the freedom from repeated visits to each measurement site should make it possible to monitor tens or hundreds of thousands, instead of hundreds, of locations.

[1] Minutes of the Meeting of the Committee on Geodesy, National Research Council, National Academy of Sciences, Washington, D.C., January 11, 1989.

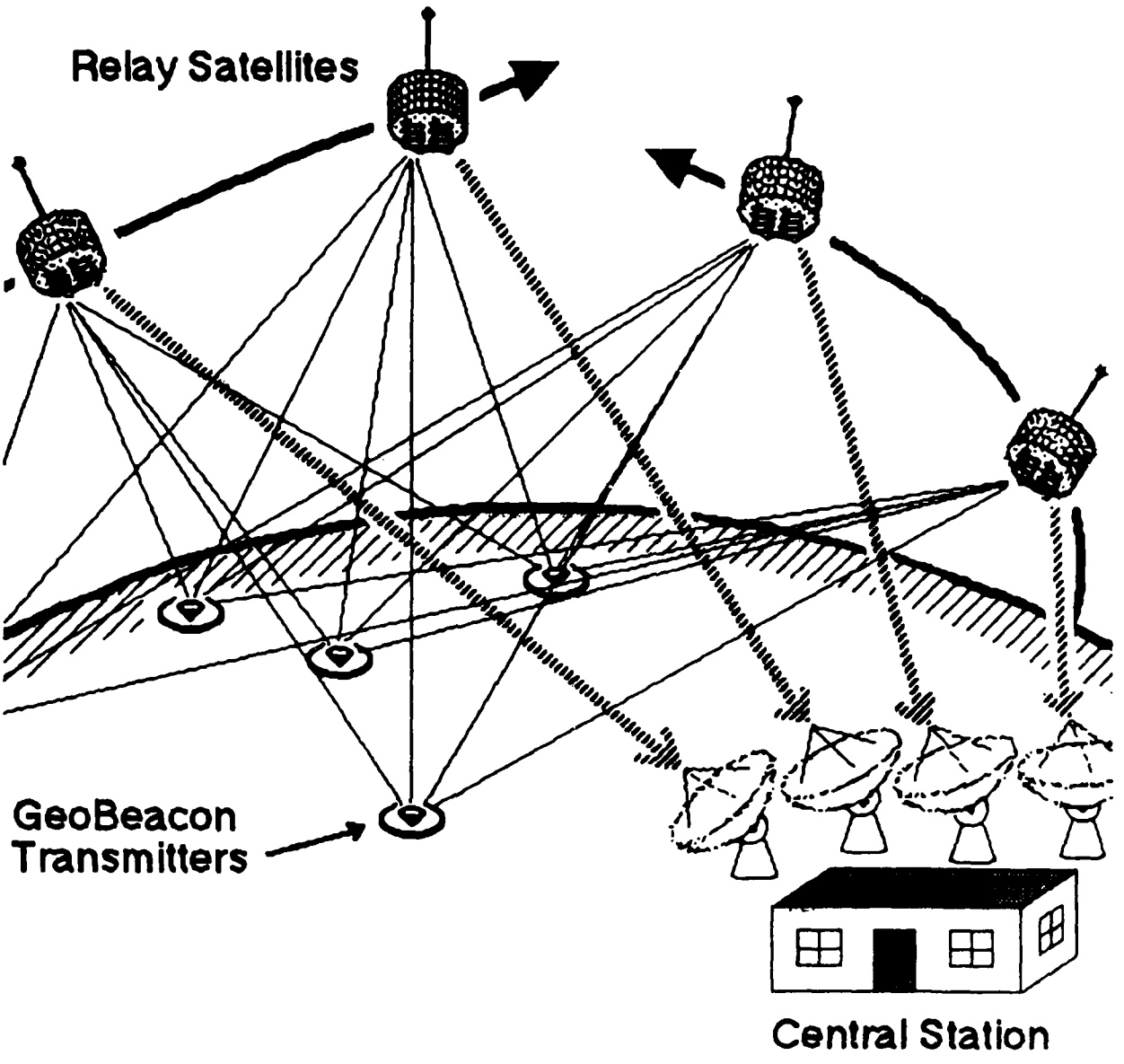

Figure 3. Overview of "GeoBeacon" Satellite Positioning System

What other possible uses does this system offer? Since the measurements are made and results are obtained at a central site, real time results for most users may not be practical. This system is not intended to replace GPS, but its different arrangement opens the opportunity for applications other than cheaper geodetic measurements. Anything can be tracked so long as a transmitting signal can be received by the observing constellation of

satellites. For instance, with pseudo-random codes used to minimize detection by an enemy, the system could be used to track troop movements. Transmitters could be timed to transmit only at certain times in order to minimize the possibility of detection, or to take advantage of energy sources (e.g. the moving wheel of a car, the ignition of a motor, etc.) Although few applications require the precision of geodetic measurements, this new system can be designed with geodetic level accuracy as its primary goal, and still allow the opportunity of tracking other objects. Unlike GPS, the GeoBeacon can furtively monitor objects, which could be an asset to surveillance groups. By giving each transmitter a unique coded message, one could recover the positions of all transmitters, and distinguish transmitters of different projects. Therefore, this system could simultaneously perform geodetic measurements and track an emergency beacon from a mountain climber.

In addition to these positioning projects, this new system could make it possible to monitor electron concentrations throughout different slices of the ionosphere, which could aid in ionospheric studies. By transmitting a signal on two linearly polarized antennas at right angles to each other, one could measure the amount of Faraday rotation of the signal. The magnitude of Faraday rotation is proportional to the path electron density. More importantly, the low transmitter cost would make it easy to place more transmitters on the Earth's surface to monitor changes of signal phase due to the ionosphere. Knowledge of this ionospheric contribution would aid in processing data for this system or any other satellite positioning system (including GPS).

These practical tracking, positioning, and measuring opportunities, which are physically and economically unattainable by GPS alone, will make this satellite positioning system worthwhile and cost effective. Therefore, this study will address the feasibility of using a low-power transmitter operating at several selected frequencies for locator and tracking purposes. This study will focus on the estimation of the required transmitter power and the frequency selections which would provide effective service for the applications mentioned.

The following section outlines the assumed needs of the users of the new system, introduces possible orbit configurations for the satellite constellations, and reviews the parts of a radio positioning system.

The power budget section examines the requirements of the radio link (eg., SNR, antenna gains) and relates them to the transmitter power need for the uplink. The objective of this section is to effectively demonstrate to a system designer what factors predominate the uplink power requirements for signal acquisition and tracking at different frequencies.

The frequency selection segment reviews the models and assumptions used for choosing the system frequencies. The goal of this section is to provide an algorithm for the system designer to follow in selecting the desired frequencies, such that information obtained from measurements at each frequency is being used to the fullest in acquiring and tracking signals at other frequencies.

Following these discussions are an analysis of results and conclusions for the estimated transmitter power and frequency selection method. Finally, this study includes recommendations for improving the models used and a possible experiment to simulate this positioning system

2. Development of Prototype System Design

2.1. Definition of User Needs

Although it is not possible to anticipate the performance requirements of every user of this new system, for this feasibility study their needs will be divided into two groups. One group will not require precision positioning, but instead will need positioning updates at intervals on the order of a few hours and most importantly, the lowest possible transmitter power. Locator systems such as an emergency SAR network would be an application with these needs. The second group will have a high precision positioning requirement (1 part in 10^9 accuracy in baseline measurements), but will only require updates on the order of once a month. These would be the needs of a crustal motion project.

To fulfill the requirements of both groups, a wide range of frequencies must be used in the positioning system. As will be demonstrated later, frequencies used in the COSPAS-SARSAT system lead to smaller path losses than the frequencies used in GPS. The lower limit on frequency selection arises from the increasing possibility that the uplink signal will become totally reflected by the ionosphere as transmitter frequency decreases. Therefore, a lower frequency bound of 100 MHz is assumed for this study. While frequencies between 100 MHz and 1 GHz have proved to be effective for SAR missions, ionospheric phase scintillation at frequencies below 1 GHz make phase prediction and tracking difficult. As will be shown later, the precision in satellite geodesy comes from tracking the carrier phase instead of the transmitted code. Also, position determination precision tends to increase with shorter wavelengths, as will be shown. Therefore, frequencies above 1 GHz must also be considered for performing geodetic measurements.

The strategy by which both types of services will be performed is as follows. The lowest frequency will most likely be the selection used for SAR. In addition to this role,

geodetic signals acquired at this allocation will be used to predict the frequency shift of the next highest frequency. Once the second frequency is tracked, information from both frequencies will be used to acquire and track the signal at the next highest frequency, and so on. Once the frequency selections exceed 1 GHz, both frequency and phase predictions of the signal will be made, for it is the phase measurements of the frequencies above 1 GHz which are relevant towards geodetic measurements.

2.2. Possible Satellite Constellations

Two scenarios were considered for this new satellite system. The first assumed that the system would be used primarily to conduct geodetic campaigns, thus eliminating the need for global 24-hour coverage. The satellite constellation that evolved from this scenario was eventually discarded. However, the constellation will be presented below in order to demonstrate how many satellites are actually needed to perform geodetic measurements as opposed to real time positioning. The second scenario reflects the requirement of continuous global coverage for vehicle tracking and rescue operations.

2.2.1. Geodetic Requirements

If this system were to be used for geodetic purposes only, the satellite configuration would not be driven by the same factors that influenced the design of the GPS configuration. The major difference is that global 24-hour coverage would not be required. In fact, a specific baseline would require a pass only on the order of once a week to once a month, since the goal of this system is to accumulate static measurements over a period of time on the order of decades. At least four satellites would be needed to minimize errors due to oscillator instabilities. The Position Dilution of Precision (PDOP) is roughly the inverse of the tetrahedral volume defined by the tips of the unit vectors toward the satellites[1], so a good distribution across the sky is required. If the satellites are placed too far apart, however, then the observation time per baseline as well as the maximum baseline length decreases, thus forcing a tradeoff between observation time (accuracy) and baseline length (system usefulness). One result considered was to have four satellites in circular

[1]Spilker Jr., J.J., pp. 32-33.

orbits, at the same altitude with varying inclinations, longitude of ascending node, and time of perigee passage:

Satellite #	a(km)	e	i(°)	Ω(°)	ω(°)	t_{cp}(s) (time of ascending equator passage)
1	32177.	0.0	45.0	0.0	0.0	1000.0
2	32177.	0.0	48.0	-4.0	0.0	0.0
3	32177.	0.0	48.0	4.0	0.0	1000.0
4	32177.	0.0	45.0	0.0	0.0	0.0

Table 1. Orbital Elements for a Geodesy-Only Positioning System

A fifth backup satellite can be placed among the four satellites. The resulting constellation guarantees that there will be no ambiguity in resolving the vertical position component, since one satellite will always be at a different elevation angle from the other three when seen from locations near the Earth's surface. The resulting footprint (area covered by all four satellites simultaneously) is roughly 11500 km in diameter. For the orbits listed above (16 sidereal hr orbits), this footprint permits observations of baselines up to 9500 km long for up to one hour. Circular orbits were chosen over elliptical paths in order to minimize PDOP variations with respect to user location.

2.2.2. Continuous Global Coverage

Since the intent of this system is to provide positions for thousands of sites in a manner unattainable by GPS, it is conceivable that both systems could be merged on a future generation NAVSTAR/GPS satellite. The positioning and ionospheric measuring

capabilities of this new system would be of interest to the military. In addition, with projected lifetimes of current navigation systems such as Omega reaching 2005[1], GPS can be expected to have a operating lifetime over several generations of GPS satellites. With that scenario in mind, the design will assume a GPS-style constellation of 18 repeater satellites orbiting at an inclination of 55 degrees in 12-sidereal hour orbits.

[1] Wenzel, Omega Navigation System - A Status Report, pp. 309-315.

2.3. GeoBeacon Transmitter

One objective of this system is to provide a relatively inexpensive means of positioning and/or tracking of thousands of sites. As mentioned earlier, by having transmitters instead of receivers at the sites of interest, the need to visit individual sites to recover information in receiver memory has been eliminated. This will lower the number of man-hours needed to conduct large surveying campaigns. The system is meant to minimize transmitter power and frequency stability requirements. With a total power requirement on the order of a watt, these site transmitters can run on solar cells charging a battery pack.

The design calls for a crystal oscillator to be used as a frequency standard, as with the emergency transmitters used in the SARSAT system. Higher-stability frequency standards, such as an atomic standard, will only be required at the central processing sites.

With their energy self-sufficiency and low cost, these transmitters can be considered disposable. That is, once the transmitter's working lifetime is exceeded, it can be replaced without burdening the resources of the user. For the geodetic user, the transmitter can be considered a cheap source of frequency and phase by which site location can be determined. For the vehicle tracker, the transmitter can be considered a cheap source of coded signals. Since every transmitter could be given its own individual wideband (~1 MHz) pseudo-random code, unauthorized detection and/or jamming, as well as unintentional interference can be avoided. A block diagram of a possible emergency locator transmitter, operating at the emergency channel of 121.5 MHz, with a 1 MHz code repeated every second, could appear as follows:

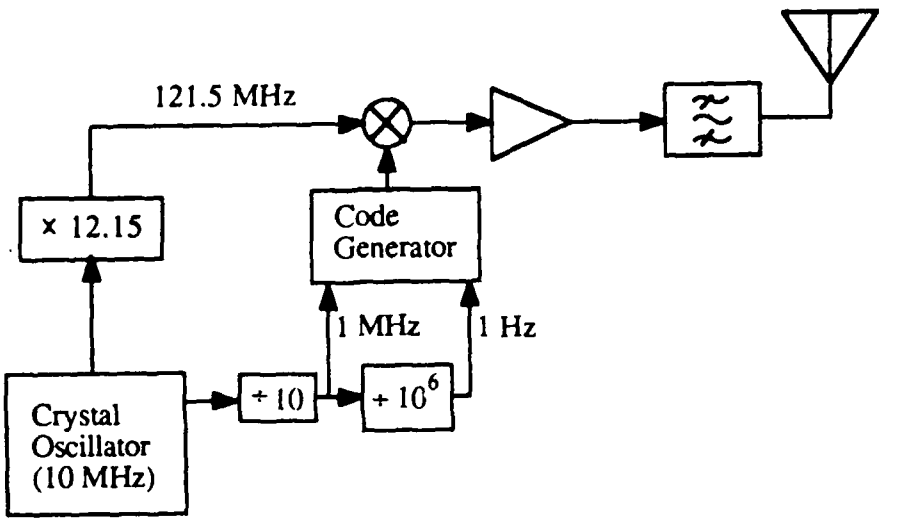

Figure 4. Emergency Locator Transmitter Block Diagram

2.4. Signal Acquisition

After the satellites have received, amplified, and re-transmitted the signal, tracking stations receive the combined signal. A block diagram of part of a receiver which would recover phase information at 1 GHz is shown. This receiver can create and store up to 10^6 complex phasor values of the received phase every second.

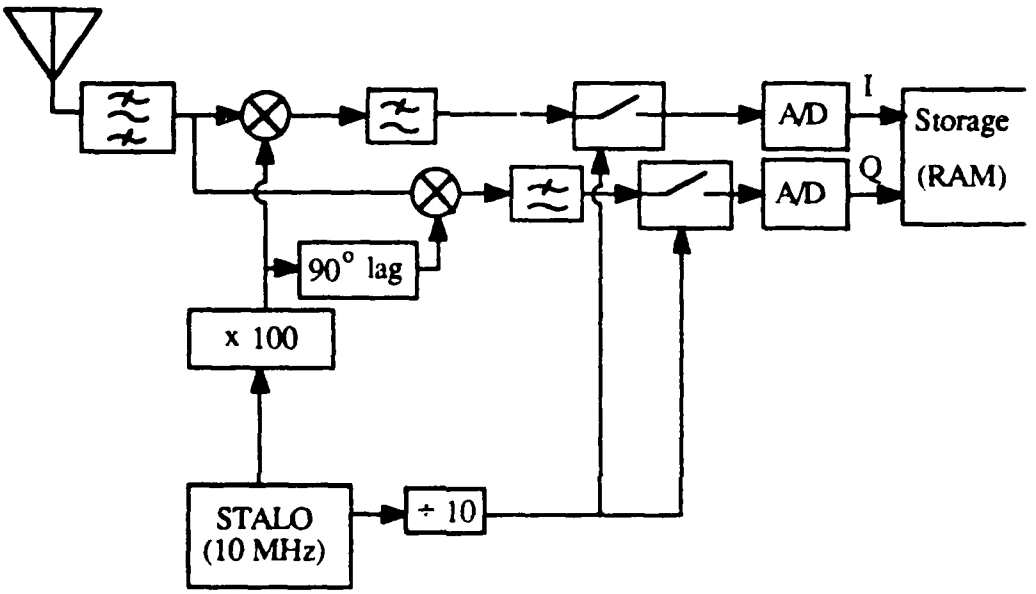

Figure 5. Portion of Receiver Block Diagram

2.5. Signal Processing

The objective of a coded signal receiver is to obtain the time difference between the received code and a reference copy of the code in the receiver. For geodetic precision the receiver's aim is to obtain the phase difference between the carrier of the received signal and a reference oscillator at the same frequency. The portion of the receiver which obtains this phase difference from the stored complex phase values is shown below. The received signal is discretely correlated with the receiver's copy of the code. Then the peak magnitude of the resulting complex values is found. If this value is not above the noise threshold, then the estimate of the carrier frequency offset (δ) must be recalculated. If the value is above the noise threshold, then one may safely assume that the time delay (phase of the code) has been found. The angle of the complex correlation value at that time is the carrier phase.

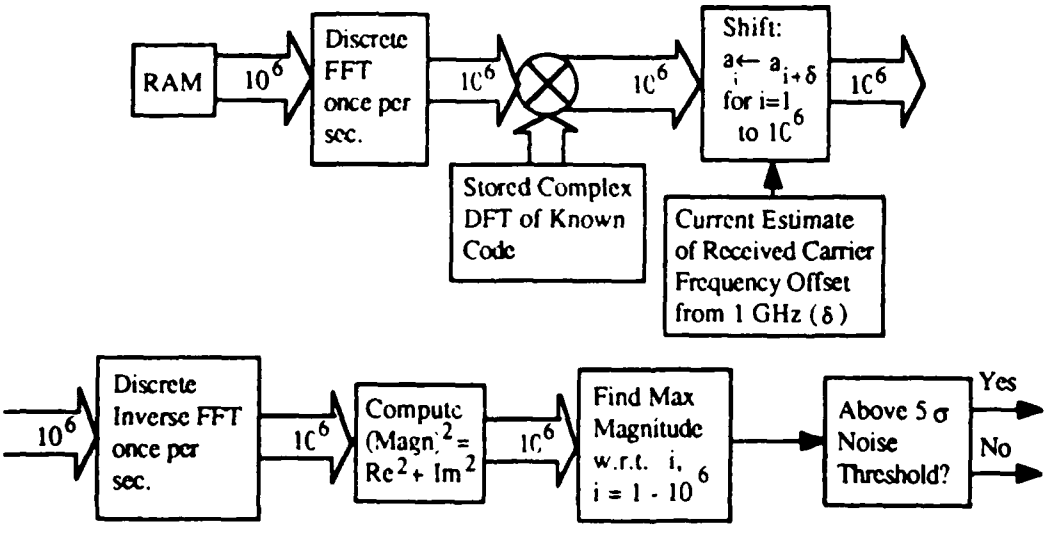

Figure 6. Remainder of Receiver Block Diagram

2.6. Baseline Determination and Measurement Resolution

In order to make a baseline measurement, techniques such as double differencing of the observable are used, and will not be covered here.[1] The following discussion demonstrates the relation between carrier frequency and positioning precision, which drives the need for higher frequencies in the system.

The in-phase and quadrature signals measured at both ends of the baseline are used to form a complex cross power observable at each measurement time ($S(t_i)$). Then an ambiguity function (R) is created which is a function of the measurement observable and the user's estimate of the baseline vector ($\vec{b}$):[2]

$$R(\vec{b}) = \left| \sum_i S^*(t_i)\hat{S}(t_i) \right| \quad (\hat{} \text{ denotes the estimated parameter}) \qquad (1)$$

By searching about 3-D space, R will yield a global-maximum value at $\hat{b} = \vec{b}$. Many details have been deliberately omitted from this procedure for simplicity, but some points need to be made about this ambiguity function. $R(\vec{b})$ is the Fourier transform of a weighted observation function. Because of this property, it follows from $R(\vec{b})$ that

i) In the new system, if the unit directional vectors from a transmitter to observing satellites define a circle on the surface of a unit sphere, the ambiguity function will degenerate to a constant value on a line perpendicular to the circle defined by the unit vectors. The 4 satellite constellation shown earlier does not suffer from this degeneracy.

ii) With GPS-satellite orbits, the ambiguity function envelope is about 2 *wavelengths* wide.

iii) With GPS-satellite orbits, the ambiguity function oscillations within the envelope have a width approximately equal to its *wavelength*.

---

[1]King, et al, Surveying with GPS.

[2]Counselman III, "Miniature Interferometer Terminals for Earth Surveying:...," pp. 245-246.

iv) Since transmissions can only be sent to the visible sky, the main peak of the ambiguity function will be about *one half wavelength* wide in any horizontal direction while it will extend *one wavelength* in the vertical direction.

v) $R(\vec{b})$, being the transform of a real-valued function, will be symmetric about the actual baseline vector ($\hat{b} = \vec{b}$).[1]

Points (ii) - (iv) demonstrate that geodetic positioning precision is proportional to frequency, justifying the need for transmitter frequencies to be as high as possible.

[1]Counselman III, "Miniature Interferometer Terminals for Earth Surveying:...," pp. 246-247.

3. Power Budgets

For this study, it is assumed that the receiving antenna for the downlink will be a dish on the order of 10 m, and the transmitting power will be about 10 w. Relative to the uplink, the downlink signal will have a much higher signal to noise ratio; therefore the study focused on the power budget for the uplink. The objective of this portion of the study is to investigate the uplink power required over the range 100 MHz - 50 GHz. As mentioned earlier, the lower frequency limit was selected due to the increasing possibility that the uplink signal would reflect off the ionosphere at lower frequencies. The upper limit was chosen since the required transmitter power is impractically high (as will be shown) at higher frequencies.

The uplink power budget defines the required power transmitted by the GeoBeacon at a particular frequency. For this study the equation defining the uplink power will be defined in dB notation for simplicity in examining each term:

$$P_T\big|_{dBw} = \left.\frac{P_R}{N}\right|_{dB} + B_S\big|_{dBHz} - G_T\big|_{dB} - G_R\big|_{dB} + P_L\big|_{dB} + L_a\big|_{dB} + L_R\big|_{dB} + M_{sys}\big|_{dB} + L_P\big|_{dB} + kT_{sys}\big|_{dBwHz^{-1}} \qquad (2)$$

where

P_T = Transmitter Power

$\frac{P_R}{N}$ = Uplink Signal to Noise Ratio (SNR)

B_S = Signal Bandwidth

G_T = Transmitter Antenna Gain

G_R = Receiver Antenna Gain

P_L = Vacuum Path Loss

L_a = Clear Atmosphere Transmission Loss

L_R = Rain Attenuation

M_{sys} = System Margin (3 dB)

L_P = Antenna Pointing Loss (3 dB)

T_{sys} = System Noise Temperature

3.1. Signal to Noise Ratio (SNR)

The accuracy of geodetic measurements made with the GeoBeacon system is proportional to the accuracy in which the carrier phase can be tracked. For this study we would like to know the carrier phase to within 0.1 radians (at 1 GHz this corresponds to 0.5 cm; at 10 GHz, 0.5 mm). To determine the minimum uplink SNR which will allow this, we must look at the phasors of the signal and noise received at the satellite. We are interested in the component of the noise phasor which is perpendicular to the signal phasor. It is this component which will change the measured carrier phase. The ratio of the lengths of the signal phasor and the perpendicular noise component for a phase error of 0.1 radians is approximately 8:1 (see figure). Since the noise phase is independent of the signal phase, the allowable electric field SNR is $8:\sqrt{2}$. The square of this ratio is the power SNR, which is approximately 15 dB.

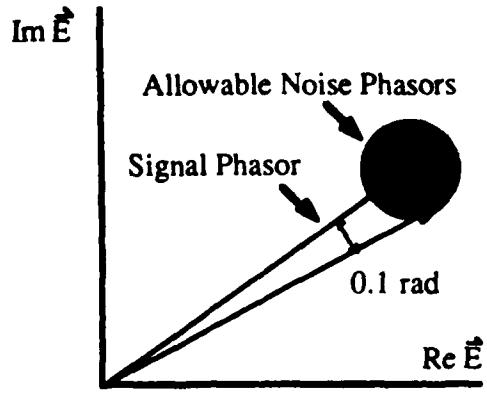

Figure 7. SNR Ratios

3.2. Integration Bandwidth

The integration bandwidth (B) is the inverse of the integration time span (t). Two sets of assumptions were made for integration bandwidth values as a function of frequency. First, for signal acquisition purposes, a value of 1 Hz was selected at 100 MHz. As will be shown in the discussion concerning frequency selection, as frequency increases, the kinematic effect upon phase increases relative to the ionospheric contribution. The integration bandwidth size will reflect the kinematic behavior as frequency increases. Since the kinematic effect upon phase is proportional to frequency, the acquisition bandwidth will increase linearly with frequency (see figure).

Once the signal is successfully acquired, this indicates that the kinematic effect upon the phase has been (hopefully) cancelled out, leaving only the ionospheric effect to change the predicted phase. The contribution of this ionospheric process to phase is proportional to the inverse of frequency, so the tracking bandwidth decreases from 1 Hz at 100 MHz to 1/30 Hz at 3 GHz. At 3 GHz the integration time is 30 s, at which point there is a risk of the signal leaving the integration bandwidth during the integration time span. Therefore, the lower limit upon tracking bandwidth is set at 1/30 Hz for frequencies above 3 GHz.

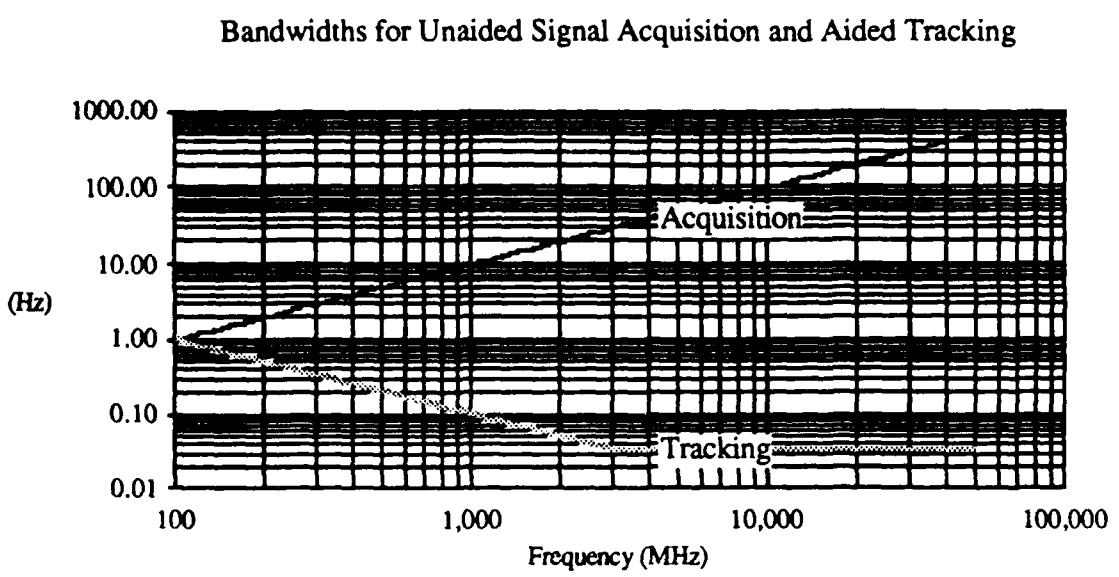

Figure 8. Integration Bandwidth

3.3. Transmitter Antenna Gain

The transmitting antenna should illuminate the whole sky, but not the ground. An antenna which had uniform gain in the upper hemisphere and none in the lower would have an upper hemisphere gain of +3 dB. In practice, the gain of an antenna must taper smoothly as a function of elevation angle, so that a realistic gain for elevations above 20° is about -2 dB.

3.4. Receiving Antenna Gain

In order to calculate the satellite uplink antenna gain, an antenna efficiency (η) of 70% is assumed, and the transmitted signal from the Earth's surface is assumed to be received at the edge of the 3 dB beamwidth. By geometry we can calculate this 3dB

beamwidth (ϕ) and the corresponding boresight gain, assuming that the satellite altitude (h) is that of a standard GPS satellite, 19700 km. The minimum allowable elevation angle (E_{min}) was chosen to be 20°, since it is difficult to find many locations on the Earth's surface which allow a clear view of the sky at lower elevation angles. It also represents a tradeoff between the increased coverage area for each satellite gained with a lower minimum elevation angle and the decreased vacuum and atmospheric losses with a higher minimum elevation angle.

The receiver gain used for the power budget will be 3dB off the boresight gain, 13.3 dB.

$$\sin\left(\frac{\phi}{2}\right) = \left(\frac{R_E}{R_E + \text{Alt.}}\right) \sin\left(90^\circ + E_{min}\right) \quad (3)$$

$$G_R' = \frac{30000}{\phi^2} \text{ (empirical formula[1])} \quad (4)$$

$$G_R = \frac{G_R'}{2} \quad (5)$$

[1]Agrawal, Design of Geosynchronous Spacecraft, p.398.

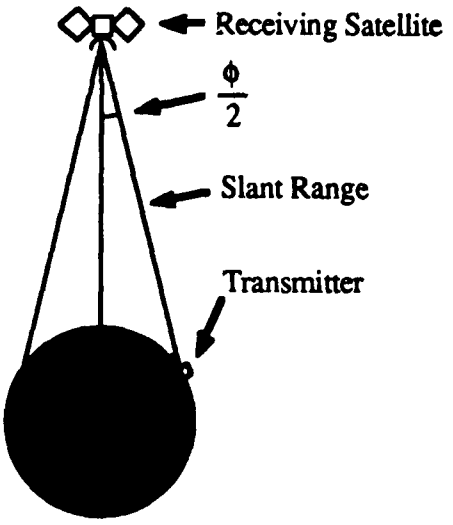

Figure 9. Receiving Antenna Gain

3.5. Path Loss

The vacuum path loss calculations for our measurements are based on the longest possible uplink slant range, which occurs when a signal transmitted from the Earth's surface at an elevation angle of 20 ^{o} to the satellite orbiting at an altitude of 19700 km. The path length (R) is found to be 23200 km. As a result of this path length assumption, the vacuum path loss is simply a function of transmitter frequency:

$$P_L = \left(\frac{4\pi Rf}{c}\right)^2 \quad (6)$$

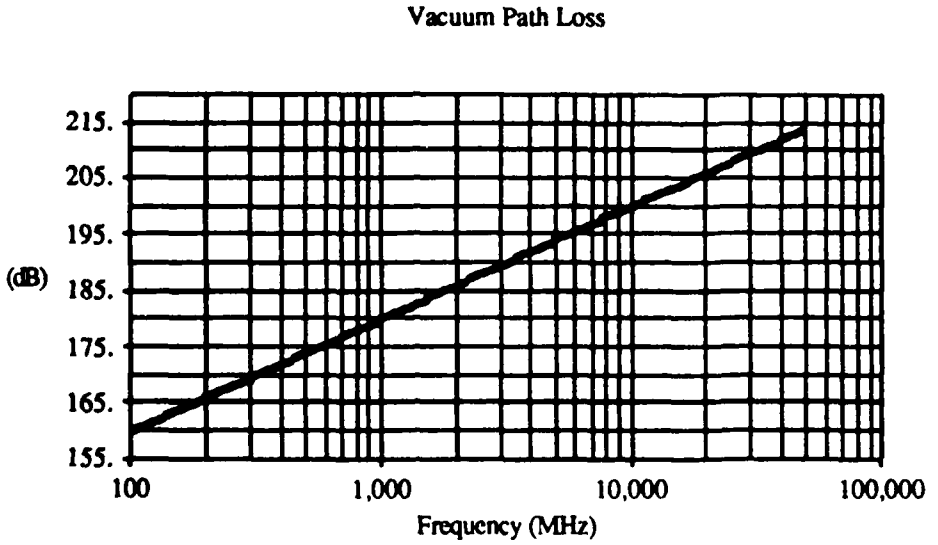

Figure 10. Vacuum Path Loss (P_L)

3.6. Atmospheric Signal Attenuation

In the frequency range being considered for this design, the principal mechanism by which radio waves are attenuated is molecular absorption. In the Earth's atmosphere two major gases have resonance frequencies in the range of interest (100 MHz - 50 GHz), water vapor and oxygen. Global samples have been taken of the contributions of water vapor and oxygen towards radiowave attenuation as a function of temperature and surface water vapor concentration (humidity).[1] The specific attenuation from these two gases, γ_a, can be calculated as a function of surface temperature and water vapor concentration:

$$\gamma_a = a(f) + b(f)\rho_o - c(f)\, T_o, \quad \text{dB/km} \qquad (7)$$

[1]Ippolito, Radiowave Propagation in Satellite Communications, p.25.

The integral of the specific attenuation over the entire slant path through the atmosphere yields the total atmospheric attenuation, A_a, which is a function of elevation angle θ:

$$A_a(\theta) = \int_0^{r_o} \gamma_a(r)\, dr, \quad dB \qquad (8)$$

Estimates of the total zenith attenuation ($A_a(90^o)$) can also be calculated from a second set of coefficients derived from a regression analysis by Crane[1]:

$$A_a(90^o) = \alpha(f) + \beta(f)\rho_o - \xi(f)T_o, \quad dB \qquad (9)$$

The algorithm for calculating the total atmospheric attenuation as a function of temperature, frequency, surface water vapor density, and elevation angle is as follows:

i) Calculate specific attenuation γ_a as a function of f, ρ_o, T_o.

ii) Calculate total zenith attenuation $A_a(90^o)$ as a function of f, ρ_o, T_o.

iii) Calculate scale height H_a, $H_a = \dfrac{A_a(90^o)}{\gamma_a}$ (10)

iv) Calculate total one-way atmos. atten. $A_a(\theta)$, $A_a(\theta) = \dfrac{H_a A_a(90^o)}{\sin\theta}$ (11)

The resulting variation of atmospheric attenuation with respect to frequency is shown below. Note the effect of the water vapor resonance at 22.3 GHz and the oxygen resonance as 60 GHz is approached.

[1]Ippolito, pp. 29-36.

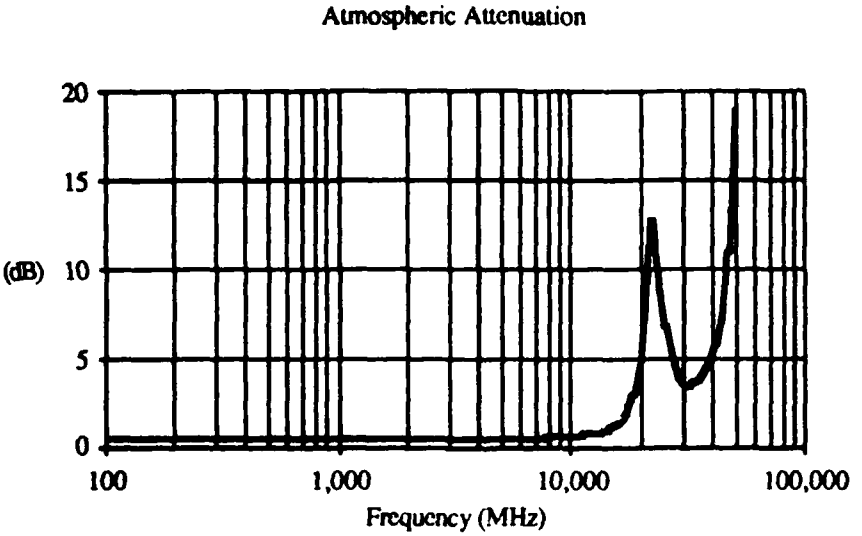

Figure 11. Total One-Way Atmospheric Attenuation (L_a)

3.7. Rain Attenuation

Attenuation of the uplink signal due to rain was not considered in the design. As shown in the previous section, rain attenuation is significant only at the higher frequencies being considered (f > 20 GHz). The most intense cases of precipitation have time spans on the order of a few hours and are localized in nature. Therefore, the geodetic capabilities of this system would not suffer appreciably. For the same reason, the system's emergency locator capability would hardly be diminished. For vehicle tracking purposes, however, the user would have to tolerate a service outages on the order of %0.01 of the year (10 hr).[1] Since tracking results will not be generated in strictly real time under ideal weather conditions anyhow, performance degradation due to heavy precipitation is not focused on in this study.

[1]Ippolito, Chapter 4.

3.8. System Noise Temperature

The effects of unwanted noise on the uplink show up in the system noise temperature (T_{sys}). The receiving antenna's 3 dB pattern will fall upon the Earth's surface, so the contributions to the noise temperature directly from the sun and from deep space will be neglected. The total noise contribution from the Earth comes from both natural and man-made sources. Due to a shortage of measurements of the radio frequency environment in Earth orbit, the estimates of natural and man-made noise carry the greatest uncertainty of any estimate in this study.

3.8.1. Natural Sources

The natural radiative temperature of the Earth has basically two regimes. At frequencies below the resonances of water vapor and oxygen (~ 20 GHz), the Earth's surface temperature dominates, with an average value of 290 K. At higher frequencies, the atmosphere absorbs the surface thermal radiation and reradiates it, with an upper limit of 290 K.[1] The value of 290 K is often used for antenna temperature in uplink noise calculations, although some consider values between 60 and 240 K to be more realistic.[2] Since it is a conservative estimate, at frequencies where man-made noise power can be considered negligible, the noise temperature is assumed to be 290 K.

---

[1]Skomal, Measuring the Radio Frequency Environment, Chapter 2.
[2]Smith and Njoku, Proceedings, IEEE 1985 International Symposium on Electromagnetic Compatibility, pp. 318-323.

3.8.2. Man-Made Sources

The contribution to the noise environment from man-made sources come in two forms. One is accidental transmission from electrically powered machinery, hereafter referred to as unintentional noise. The second form is from transmitters deliberately operating (legally or illegally) in frequency allocations assigned to this new system. This type of noise will be referred to in this study as deliberate transmitter noise.

There is a growing need, which has been recognized by the international communications satellite community, to measure and control the amount of man-made electromagnetic interference to radio links both on Earth and in Earth orbit. Since insufficient measurements of man-made radio emissions to outer space exist over the 100 MHz - 100 GHz range of the spectrum, estimates must be made of the expected noise level.

Most studies addressing this topic to date have assumed the satellite to be a communications satellite at a geosynchronous altitude. Since the main lobe of the satellite receiving antenna gain pattern in this design will also fall within the Earth disc, the results of these studies are relevant.

3.8.2.1. Unintentional Man-Made Noise

A study conducted by Skomal[1] assumed that the impulsive contributions to this incidental noise power $p_h(f)$ from consumer products, automotive ignition systems, industrial equipment and electric-power generation resembled thermal noise in nature at great distances.

$$p_h(f) = \frac{A_r Q}{4\pi A_m} \int_A \frac{p_n(f,d) F(\gamma_1,\gamma_2) dA}{R^2} \quad (12)$$

where

A_r = Antenna Effective Area

$F(\gamma_1,\gamma_2)$ = Normalized Antenna Power Pattern (function of two direction angles)

A_m = Tuned Dipole Effective Area

Q = Receiving Antenna Polarization Factor
(linear polarization = 1, circular polarization = 2)

$p_n(f,d)$ = Incidental Noise Surface Dist. (function of frequency, source dimension)

Skomal proposed that most unintentional man-made noise comes from metropolitan areas, and that their contributions can be modeled and summed to yield the total incidental noise power:

$$p_h(f) = l \frac{Q g_d}{8\pi^2} \sum_{i=1}^{I} \langle p_n(f,d_i) \rangle_i \, \Omega_i \quad (13)$$

[1]Skomal, IEEE Transactions on Electromagnetic Compatibility, pp. 321-328.

$$l = \int_{\theta_1}^{\theta_2} d\theta \int_{\phi_1}^{\phi_2} d\phi \frac{\sin\theta \cos\phi \left[1 - 1/2 \left(\frac{kar_o}{2R_i} \right)^2 (1-\sin^2\theta \cos^2\phi) \right]}{(R_i/h)^2} \quad (14)$$

where

g_d = Antenna gain relative to a tuned dipole

Ω_i = Solid angle subtended by i^{th} class urban area at altitude h

$\langle p_n(f,d_i) \rangle_i$ = Ave. Surface Noise Power for urban area with radius d_i

The urban area is assumed to be circular, and the surface noise power is obtained from ξ_i which are frequency dependent:

$$p_n(f,d_i) = b\, 10^{0.1 \sum_{j=1}^{3} \xi_i (d-2.5)^{j-1}} \quad (15)$$

yielding

$$\langle p_n(f,d_i) \rangle_i = \frac{bN_i}{A_i} \int_0^{2\pi} d\theta \int_0^{d_i} d\, 10^{0.1 \sum_{j=1}^{3} \xi_i (d-2.5)^{j-1}} d(d) \quad (16)$$

The distribution of urban areas for the Western Hemisphere was tabulated, along with their characteristic dimensions:

Index	Population	$\langle A_i \rangle$	d_i	Ω_i	Number of Cities (1970), N_i		
(i)	($\times 10^{-3}$)	(sq mi)	(mi)	(sr $\times 10^{8}$)	USA	N.Amer.	W.Hemisphere
1	10-49.9	14.2	2.13	3.29	515	540	1080
2	50-99	24.2	2.78	5.61	223	233	393
3	100-299	45.4	3.80	10.5	106	109	219
4	300-499	124	6.29	28.9	23	25	49
5	500-999	194	7.85	44.9	19	20	34
6	1000-2999	291(sic)	9.62(sic)	67.5(sic)	4	4	10
7	>3000	261(sic)	9.12(sic)	60.6(sic)	2	2	4

Table 2. Distribution of Urban Areas by Population

The coefficients (ξ_i) can be found by the simultaneous solution of three equations given in Skomal and Smith:

$$\text{i)} \left[\delta P_s(f,\bar{d})/\delta d\right]_{\bar{d}=0} = 0, \text{ using } P_s(f,\bar{d}) = \xi_1 + \xi_2(\bar{d} - \bar{\kappa}) + \xi_3(\bar{d} - \bar{\kappa})^2 \qquad (17)$$

$$\text{ii)} \left[P_s(f,\bar{d})\right]_{\bar{d}=2.5 \text{ miles}} = P_a, \text{ using the urban composite noise function}$$

$$P_a = -21.8 - 12.2 \log_{10} f \qquad (18)$$

$$\text{iii)} \left[P_s(f,\bar{d})\right]_{\bar{d}=10 \text{ miles}} = P_a, \text{ using the suburban composite noise function}$$

$$P_a = -8.7 - 14.5 \log_{10} f \qquad (19)$$

The resulting estimated unintentional man-made noise power spectral density is shown in the figure below. This estimate assumes that the satellite is over North America; it is reasonable to believe that there is no other location over the Earth's surface where the level of interference noise will be greater.

3.8.2.2. Deliberate Transmitter Noise

In a study conducted by Birch and French[1], a compilation was made of all the power emitted from licensed transmitters over the frequency range 117-155 MHz. Their transmitter information sources included the IFRB (International Frequency Registration Board), the ECAC (Electromagnetic Compatibility Analysis Center), and Jeppesen Air Manuals. From this information a program was used to estimate the noise power density received by a geosynchronous satellite at a longitude where the expected noise power would be relatively high compared to other longitudes.

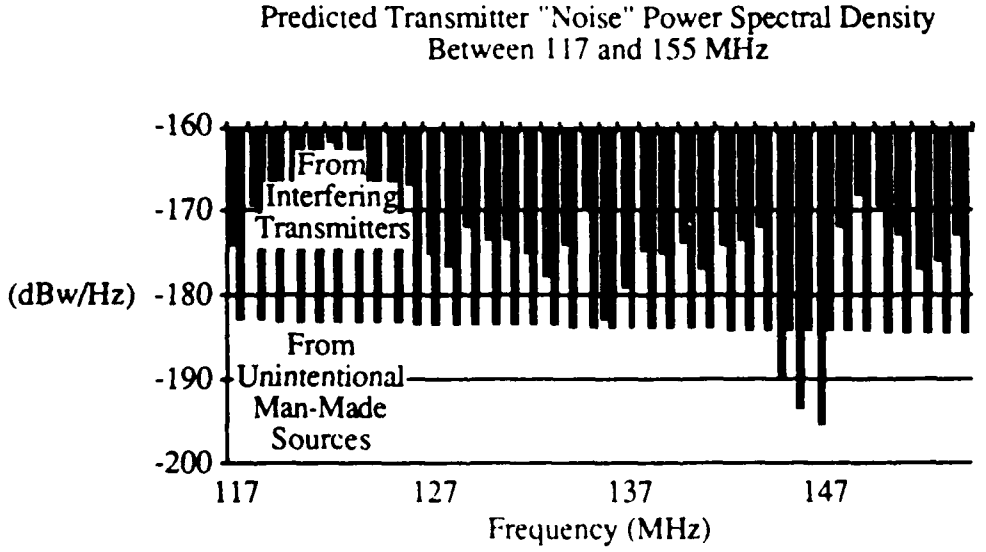

Figure 12. Predicted Transmitter Noise Power Density

(from geosynchronous orbit at 143° W. Long.)

[1]Herman, IEEE 1978 International Symposium on Electromagnetic Compatibility, pp. 339-346.

The frequency allocations of this frequency range are listed below[1]:

1) 117 - 118 MHz: Aeronautical Radionavigation
2) 118 - 136 MHz: Aeronautical Mobile
3) 136 - 137 MHz: Aeronautical
4) 137 - 138 MHz: Space Operation, Space Research Service, Meteorological - Satellite Service (all Space to Earth)
5) 138 - 143 MHz: Aeronautical Mobile
6) 143 - 144 MHz: Space Research
7) 144 - 146 MHz: Amateur, Amateur Satellite
8) 146 - 150 MHz: Fixed Service
9) 150 - 155 MHz: Fixed Mobile Services

When the estimated incidental noise density is included with the predicted transmitter noise density, it appears that on the average man-made transmitter noise increases the noise density by 10 dB. When this system is implemented there is no guarantee that it will be allocated frequency bands with little interference noise, such as the amateur radio band (region 8 above). These predicted estimates will probably increase with time as the number of transmitters increases. As a result of these predictions, the man-made transmitter noise power density is assumed to be 10 dB above the level estimated for interfering noise (see Figure 13).

[1] ITU Radio Regulations.

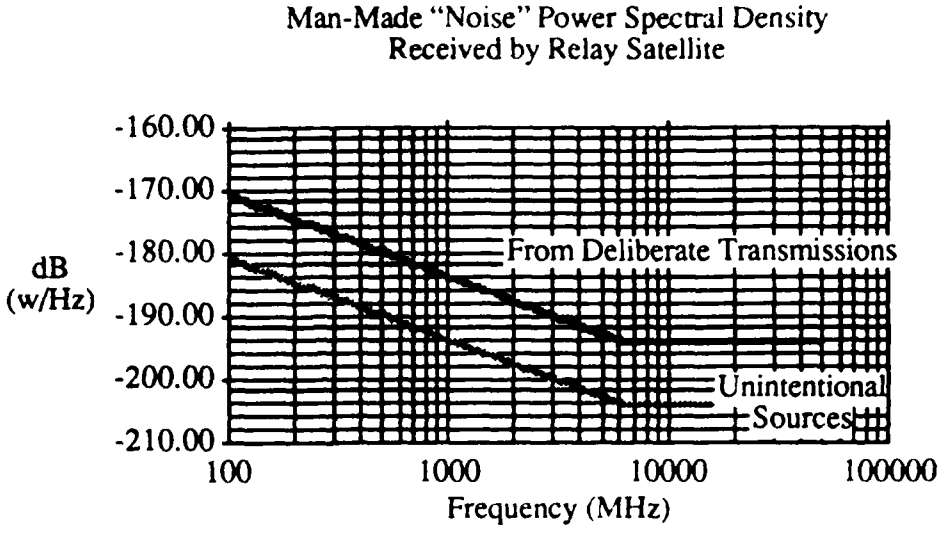

Figure 13. Total Man-Made Noise Power Density Assumption

3.8.3. International Frequency Allocation Need

No measurements of the actual radio noise levels from transmitters at GPS-orbit altitudes were available. However, one can calculate the amount of transmitter noise which can be tolerated at any particular frequency bandwidth. The estimates shown below demonstrate that the new system cannot share its frequency allocations with commercial radio broadcasters or microwave link users. Therefore, there may be a need to reserve frequency allocations for this new system, as was done for the COSPAS-SARSAT and GPS systems.

For the case of a satellite receiving interference from a ground transmitter, an interference-free link must satisfy the following power relation:

$$P_i\big|_{dBw} \geq$$

$$P_e\big|_{dBw} + G_e\big|_{dB} + G_R\big|_{dB} + \left.\frac{\Delta F_r}{\Delta F_c}\right|_{dB} - P_L\big|_{dB} - D_p\big|_{dB} - A_o\big|_{dB} - D_f\big|_{dB} - A_n\big|_{dB}(\epsilon) \qquad (20)$$

where

P_i = Permissible Interference Power Level

P_e = Interfering Transmitted Power

G_e = Transmitting Antenna Gain in direction in question

G_r = Satellite Receiver Antenna Gain in Direction in Question (13.27 dB)

$\frac{\Delta F_r}{\Delta F_e}$ = Receiving/Interference Bandwidth Ratio. (0 dB for most conservative case)

P_L = Vacuum Path Loss of Interfering Signal

D_p = Polarization Losses Due to Transmitter - Receiver Mismatch (0 dB; most conservative case)

A_b = Receiver Connection Losses (0 dB; most conservative case)

D_f = Frequency Decoupling (0 dB; most conservative case)

$A_h(\varepsilon)$ = Losses due to Horizon Relief (0 dB; most conservative case)

Two cases are considered: a commercial FM radio transmitter and a microwave relay link.

A) FM Transmitter (100 MHz):

As per the discussions of vacuum path loss and noise power earlier, at 100 MHz we assume P_L = 160.5 dB and P_i = -172 dBwHz^{-1} + 60 dBHz = -112 dBw (for a 1 MHz coded signal). The antenna gain is assumed to be independent of azimuth with a 3 dB beamwidth between elevation angles of 0^o and 1.8^o. Therefore, G_e is about 12 dB. The resulting power relation is

$$P_e\big|_{dBw} \leq -112 \text{ dBw} - 12 \text{ dB} - 13.27 \text{ dB} + 160.5 \text{ dB} - 0 \text{ dB}$$

$$P_e\big|_{dBw} \leq 23.23 \text{ dBw} \rightarrow 210 \text{ w}$$

At 10 kw per transmitter, this corresponds to 0.021 transmitters over the area in view. In order to estimate the total allowable number of microwave transmitters, the main lobe beamwidth of 3.6^{o} is taken into account. The zone of interference, the annular strip of land within which the satellite is seen at elevation angles between 0^{o} and 1.8^{o} is calculated (see figure below). This area is found to be $2.4(10^{6})$ km^{2}. This corresponds to a FM transmitter density of $8.75(10^{-5})$ transmitters per 10,000 km^{2}. Therefore, this new system could not coexist with commercial FM radio.

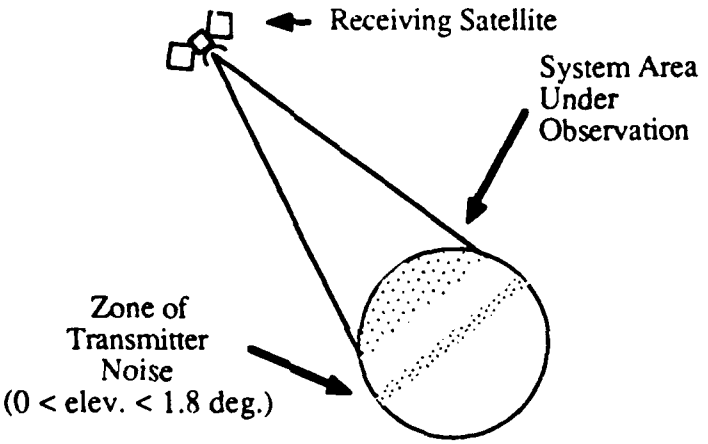

Figure 14. Location of Transmitter Noise

B) Microwave Transmitter

In order to reflect current trends in radio - relay systems, representative values for terrestrial stations have been developed.[1] At 2.2 GHz we assume P_{L} = -188 dB and P_{i} = -188 $dBwHz^{-1}$ + 60 dBHz = -128 dBw. The axial transmitting antenna gain is assumed to

[1]Annex VI, Rep. 396-5, Recommendations and Reports of the CCIR, 1986, p.160.

have a pencil beam with a main lobe 3 dB beamwidth of 3.6° and an axial gain (G_e) of 36 dB. The resulting power relation is

$$P_e\,|_{dBw} \leq -128\ dBw - 36\ dB - 13.27\ dB + 188\ dB - 0\ dB$$

$$P_e\,|_{dBw} \leq 10.73\ dBw \rightarrow 11.8\ w$$

At 13 dBw (20 w) per transmitter[1], this corresponds to 0.59 transmitters over the area in view. Over this interference zone, the pointing azimuths of these transmitters are evenly spread out over 360°. Thus, the system can tolerate 100 times more transmitters without exceeding the interference power level. This corresponds to a FM transmitter density of 0.34 transmitters per 10,000 km^2 (the assumed density is currently 5 transmitters per 10,000 km^2). Therefore, fixed radio - relay allocations would lend themselves more than the commercial FM band to the possibility of frequency sharing with this new positioning system. Nevertheless, the level of noise interference in this case is over 10 times the amount tolerable by the new system. There will be a need to study the feasibility of frequency sharing for the new system at other frequency allocations.

[1] Ibid.

4. Frequency Selection

As it was shown in section 2.6, the precision of geodetic measurements improves with decreasing wavelength. One could perform high precision geodesy with a transmitter operating at one relatively high frequency (f > 10 GHz). However, it would require a prohibitively large amount of power to acquire and track the signal at this high frequency.

There is another method by which signals at high frequencies can be accurately tracked. Let the transmitter transmit signals at two frequencies, one high and one low, both being derived by multiplication from the same oscillator so that the ratio of the frequencies is a known constant. One first acquires and tracks the low frequency signal. Having measured the frequency of this signal, one multiplies the measured value by the known ratio to obtain a prediction of the higher received frequency. This prediction will have an error, due to (1) error of measurement of the lower frequency, and (2) ionospheric effects, which are not proportional to frequency. This prediction error limits how far up in frequency one can go and still expect to acquire a signal within one's tracking bandwidth (discussed in section 2.6). Measurements at thie higher frequency may be used in acquiring a third frequency, and so forth, until one can acquire and track signals at frequencies necessary for geodetic work. The power needed to transmit the higher frequencies is that required for aided tracking instead of the power needed for unaided acquisition. Thus, "bootstrapping" one's way up to the desired frequency results in a lower total power required in tracking a high frequency signal.

To help in deciding how to calculate the frequency intervals, a model must be created which accounts for the different contributions to the errors of the measured frequencies. The model is then examined to see how errors of the higher-frequency predictions vary with time and with additional measurements. After this behavior has been modeled, a Kalman filter can be used to simulate the effects of real time measurements upon the state estimate covariances. Once we know how accurate our estimates will be for

a particular set of frequencies, we can extrapolate our estimate of phase and frequency until we meet a pre-established criterion at the next highest frequency.

The basic measurements this system relies upon are those of phase and frequency. These observables have frequency dependent contributions from the system kinematics and the ionosphere. By kinematics we refer to the motions of the transmitter and the receiving satellite as well as the drift in the transmitter crystal oscillator and receiver data processor frequency source. The kinematic effect upon phase and its time derivatives (frequency, frequency drift rate, etc.) is directly proportional to frequency, whereas the ionospheric effect is inversely proportional to frequency. In equation form phase (ϕ) and frequency ($\dot{\phi}$) appear, respectively, as

$$\phi = A\,f + B\,f^{-1} \quad \text{and} \quad \dot{\phi} = \dot{A}\,f + \dot{B}\,f^{-1} \qquad (21, 22)$$

4.1. State Space Model

The kinematic and ionospheric processes have different effects upon the two types of measurements as the frequency is varied. In order to investigate further, a state vector ($\underline{x}$) and measurement vector ($\underline{y}$) were defined as follows:

$$\underline{x}^T = \left[x_1\ x_2\ x_3\ x_4\ x_5\ x_6\right]^T = \left[A\ \dot{A}\ \ddot{A}\ B\ \dot{B}\ \ddot{B}\right]^T$$

$$\underline{y} = \left[\phi_1\ \dot{\phi}_1\right] \text{ (measurements at one frequency)}$$

The kinematic and ionospheric second time derivatives, $\ddot{A}$ and $\ddot{B}$ respectively, are modeled as Gauss-Markov processes. This choice reflects the assumption that these processes are random, but that their present values are exponentially correlated with past and future values with a time constant β^{-1}.

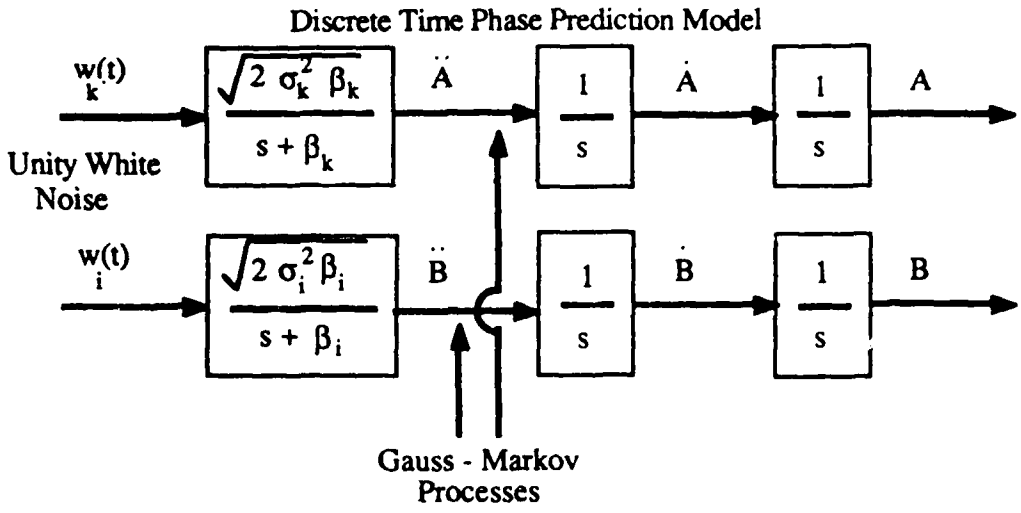

Figure 15. Integrated Gauss-Markov Processes

The state-space description of these processes is

$$\dot{\underline{x}} = F\,\underline{x} + G\,\underline{w} \qquad (23)$$

$$\underline{y} = B\,\underline{x} \qquad (24)$$

where F and the observation matrix B are given as

$$F = \begin{bmatrix} 0 & 1 & 0 & & & \\ 0 & 0 & 1 & & & \\ 0 & 0 & -\beta_k & & & \\ & & & 0 & 1 & 0 \\ & & & 0 & 0 & 1 \\ & & & 0 & 0 & -\beta_i \end{bmatrix} \quad B = \begin{bmatrix} f_1 & 0 & 0 & f_1^{-1} & 0 & 0 \\ 0 & f_1 & 0 & 0 & f_1^{-1} & 0 \end{bmatrix}$$ (again, measurements at one frequency)

Since our measurement process is digital, we assume discrete measurements of phase and frequency taken at constant time intervals. The discrete time estimate of the state vector based on an estimate at a prior time can be made with the discrete state transition matrix (Φ_k).

$$\hat{\underline{x}}_k = \Phi_{k-1}\,\hat{\underline{x}}_k + \underline{w}_{k-1} \quad (\underline{w}_{k-1} \text{ is a process noise } \textit{vector}, \neq w_k, w_i) \qquad (25)$$

The entries of the discrete state transition matrix, Φ_k, can be calculated from the kinematic and ionospheric models from

$$\Phi_k = \left[L^{-1}[(sI - F)^{-1}]\right]_{t=\Delta t} \quad (L^{-1} \text{ denotes inverse Laplace transform}) \qquad (26)$$

$$= L^{-1}_{t=\Delta t}\begin{bmatrix} s & -1 & 0 & & & \\ 0 & s & -1 & & & \\ 0 & 0 & s+\beta_k & & & \\ & & & s & 1 & 0 \\ & & & 0 & s & -1 \\ & & & 0 & 0 & s+\beta_i \end{bmatrix}^{-1}$$

$$= \begin{bmatrix} 1 & \Delta t & \frac{1}{\beta_k^2}(\beta_k\Delta t - 1 + e^{-\beta_k\Delta t}) & & & \\ 0 & 1 & \frac{1}{\beta_k}(1-e^{-\beta_k\Delta t}) & & & \\ 0 & 0 & e^{-\beta_k\Delta t} & & & \\ & & & 1 & \Delta t & \frac{1}{\beta_i^2}(\beta_i\Delta t - 1 + e^{-\beta_i\Delta t}) \\ & & & 0 & 1 & \frac{1}{\beta_i}(1-e^{-\beta_i\Delta t}) \\ & & & 0 & 0 & e^{-\beta_i\Delta t} \end{bmatrix}$$

The corresponding transfer functions and weighing functions between the kinematic and ionospheric process noises are obtained from the block diagrams:

$$G_1(s) = \frac{X_1(s)}{N_k(s)} = \frac{\sqrt{2\sigma_k^2\beta_k}}{s^2(s+\beta_k)} \qquad g_1(t) = \sqrt{2\sigma_k^2\beta_k}\,\frac{1}{\beta_k^2}(\beta_k t - 1 + e^{-\beta_k t}) \qquad (27,28)$$

$$G_2(s) = \frac{X_2(s)}{N_k(s)} = \frac{\sqrt{2\sigma_k^2\beta_k}}{s(s+\beta_k)} \quad g_2(t) = \sqrt{2\sigma_k^2/\beta_k}\,(1 - e^{-\beta_k t}) \qquad (29,30)$$

$$G_3(s) = \frac{X_3(s)}{N_k(s)} = \frac{\sqrt{2\sigma_k^2\beta_k}}{s+\beta_k} \quad g_3(t) = \sqrt{2\sigma_k^2\beta_k}\; e^{-\beta_k t} \qquad (31,32)$$

$$G_4(s) = \frac{X_4(s)}{N_i(s)} = \frac{\sqrt{2\sigma_i^2\beta_i}}{s^2(s+\beta_i)} \quad g_4(t) = \sqrt{2\sigma_i^2\beta_i}\,\frac{1}{\beta_i^2}(\beta_i t - 1 + e^{-\beta_i t}) \qquad (33,34)$$

$$G_5(s) = \frac{X_5(s)}{N_i(s)} = \frac{\sqrt{2\sigma_i^2\beta_i}}{s(s+\beta_i)} \quad g_5(t) = \sqrt{2\sigma_i^2/\beta_i}\,(1 - e^{-\beta_i t}) \qquad (35,36)$$

$$G_6(s) = \frac{X_6(s)}{N_i(s)} = \frac{\sqrt{2\sigma_i^2\beta_i}}{s+\beta_i} \quad g_6(t) = \sqrt{2\sigma_i^2\beta_i}\; e^{-\beta_i t} \qquad (37,38)$$

These weighing functions can now be integrated to find the mean-square responses of the state variables to the process noises, the entries of Q_k, the process covariance matrix (see Appendix for calculation of entry values):

$$Q_k = \begin{bmatrix} E[x_1x_1]\; E[x_1x_2]\; E[x_1x_3] & & \\ E[x_1x_2]\; E[x_2x_2]\; E[x_2x_3] & 0 & \\ E[x_1x_3]\; E[x_2x_3]\; E[x_3x_3] & & \\ & E[x_4x_4]\; E[x_4x_5]\; E[x_4x_6] & \\ 0 & E[x_4x_5]\; E[x_5x_5]\; E[x_5x_6] & \\ & E[x_4x_6]\; E[x_5x_6]\; E[x_6x_6] & \end{bmatrix} \quad (E[\cdot] \text{ denotes expectation})$$

4.2. Discrete Kalman Filter

For this study we are not interested with propagating estimates and making measurements to update the state vector. Instead, we are doing an analysis of the errors of

the estimates of the state vector, the entries of the state estimate covariance matrix P_k. The basic discrete Kalman filter framework is shown below:

System Model	$\underline{\hat{x}}_k = \Phi_{k-1}\,\underline{\hat{x}}_k + \underline{w}_{k-1}\,,\ \underline{\hat{w}}_k \sim N(\underline{0},Q_k)$	(25)
Measurement Model	$\underline{z}_k = H_k\,\underline{\hat{x}}_k + \underline{v}_k\,,\quad \underline{v}_k \sim N(\underline{0},R_k)$	(39)
Initial Conditions	$E[\underline{\hat{x}}(0)] = \underline{\hat{x}}_o,\ E[(\underline{\hat{x}}_k - \underline{\hat{x}}_k)(\underline{\hat{x}}_k - \underline{\hat{x}}_k)^T] = P_o$	
Other Assumptions	$E[\underline{\hat{x}}_j \underline{\hat{x}}_k^T] = 0$ for all j,k	
Extrapolation:		
State Estimate	$\underline{\hat{x}}_k(-) = \Phi_{k-1}\,\underline{\hat{x}}_k(+)$	(40)
State Error Covariance	$P_k(-) = \Phi_{k-1}\,P_{k-1}(+)\Phi_{k-1}^T + Q_{k-1}$	(41)
Measurement Update:		
State Estimate	$\underline{\hat{x}}_k(+) = \underline{\hat{x}}_k(-) + K_k[\underline{z}_k - H_k\,\underline{\hat{x}}_k]$	(42)
State Error Covariance	$P_k(+) = [I - K_kH_k]\,P_k(-)$	(43)
Output Error Covariance	$\Sigma_k = H_kP_k(+)H_k^T$	(44)
Kalman Gain Matrix	$K_k = P_k(-)\,H_k^T\,[H_kP_k(-)H_k^T + R_k]^{-1}$	(45)

Table 3. Discrete Kalman Filter Equations

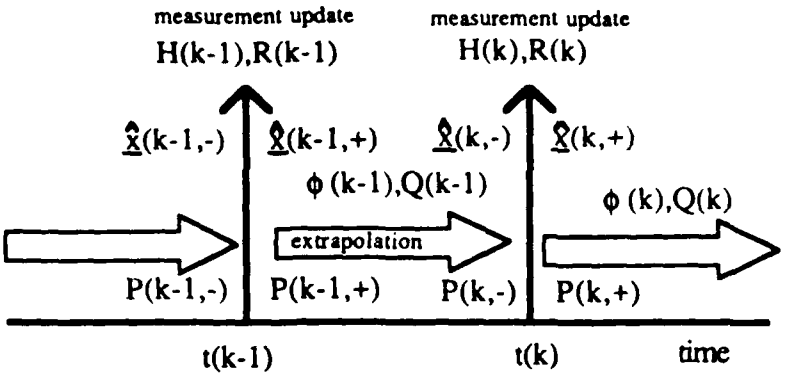

Figure 16. Discrete Kalman Filter Sequence

By iterating the Kalman filter covariance extrapolations and updates, the state covariance matrix should converge on a constant value after several measurements. After converging, the values of P_k can be used to calculate the next highest frequency which can accurately be acquired based on measurements at the lower frequencies.

In order to reduce the possibility of numerical error due to roundoff, a "square root" algorithm is recommended, that is, a square root matrix (with a smaller dynamic range than P_k) is propagated instead of P_k. (Refer to the Appendix for an outline of this algorithm, known as Potter's Mechanization of the Kalman algorithm).[1] To start the filtering, *a priori* estimates of the state vector elements are given, based on previous information, such as prior measurements or crude estimates.

The system designer should consider two trials for finding the "bootstrapping" frequencies, one for a system which performs geodesy and vehicle tracking, and a second which performs geodetic measurements only.

For the first trial for vehicle tracking capabilities, vehicle dynamics will dominate the initial estimates of kinematic errors. The initial estimates for mean position, velocity,

[1]Suggested further reading on the "Square Root" algorithm: Bierman, Gerald J., Factorization Methods for Discrete Sequential Estimation, 1977, Chapter 2, and Battin, Richard H., An Introduction to the Mathematics and Methods of Astrodynamics, 1987, Section 13.7.

and acceleration errors are to be of the magnitude encountered when tracking a land vehicle, for example:

$$\sigma_A = 3.3333(10^{-6})\ \text{s (corresponds to a 1000 m position uncertainty)}$$

$$\sigma_{\dot{A}} = 3\ 3333(10^{-8})\ \text{(-) (corresponds to a 10 m s}^{-1}\text{ velocity)}$$

$$\sigma_{\ddot{A}} = 3.3333(10^{-8})\ \text{s}^{-1}\text{ (corresponds to a 10 m s}^{-2}\text{ acceleration)}$$

Assumptions about ionospheric behavior should be made (the values below are referenced to 1 GHz):

$$\sigma_B = 3.3333(10^{5})\ \text{s (corresponds to 100 m pathlength uncertainty)}$$

$$\sigma_{\dot{B}} = 3.3333(10^{7})\ \text{(-) (corresponds to a 10 m s}^{-1}\text{ phase velocity)}$$

$$\sigma_{\ddot{B}} = 3.3333(10^{11})\ \text{s}^{-1}\text{ (corresponds to a } 10^{-4}\text{ m s}^{-2}\text{ frequency rate of change)}$$

The Gauss-Markov process noise variances and their time constants need to be approximated:

$$\sigma_k^2 = 10^{-16}\ \text{s}^{-2}\text{ (corresponds to a 0.3 g acceleration uncertainty)}$$

$$\sigma_i^2 = 1.1111(10^{11})\ \text{Hz}^4\text{s}^{-2}\text{ (corresponds to a } 10^{-4}\text{ m s}^{-2}\text{ frequency rate of change)}$$

$$\beta_k = 1.0\ \text{s}^{-1} \quad \beta_i = 0.1\ \text{s}^{-1}$$

A time interval between measurements (e.g., one second) needs to be selected, as well as the starting (lowest frequency) (e.g., 100 MHz).

For the second trial, for a system with only geodetic positioning capabilities, the ionospheric parameters remain the same. The kinematic mean error estimate of acceleration is no longer dependent upon the dynamics of the vehicle being tracked, but upon the oscillator stability. The time increments and starting frequency also remain the same. In this case the new estimates are:

$\sigma_{\dot{A}} = 2.7777(10^{-13})$ s^{-1} (corresponds to a 10^{-9} oscillator frequency drift rate per hour)

$\sigma_{\dot{A}} = 3.3333(10^{-8})$ (-) (corresponds to a 10 m s^{-1} velocity)

$\sigma_A = 3.3333(10^{-6})$ s (corresponds to a 1000 m position uncertainty)

$\beta_k = 1.3889(10^{-4})$ s^{-1} (corresponds to two hours of continuous observation by any one satellite)

The mean measurement errors (elements of R_k) are assumed to be independent between frequencies and independent between phase and frequency measurements at one transmitter frequency allocation. Therefore R_k is a diagonal matrix, and these diagonal entries are broken up into two regimes. At frequencies below 1 GHz the phase cannot be measured meaningfully (primarily due to ionospheric multipath). The assumed mean measurement errors for phase and frequency are, respectively,

$$\sigma_\phi = 1 \text{ cycle} \quad \sigma_{\dot{\phi}} = 0.2 \text{ Hz (to account for multipath)}$$

At frequencies above 1 GHz, we assume that ionospheric multipath problems have diminished. New mean measurement error estimates can be made to reflect this improvement:

$$\sigma_\phi = 0.03 \text{ cycle} \quad \sigma_{\dot{\phi}} = \frac{\sqrt{12}}{\text{Integration Time}} * \sigma_\phi$$

4.3. Selecting New Frequencies

Since we assume that phase measurements are not useful at frequencies below 1 GHz, only the frequency estimate accuracy is of concern in that regime. From the elements of Σ_k the frequency estimate variance can be written as a function of frequency:

$$\sigma^2_{\hat{\phi}} = \sigma^2_{\hat{A}} f^2 + 2\,\sigma_{\hat{A}\hat{B}} + \sigma^2_{\hat{B}} f^{-2} \qquad (46)$$

Once the variances shown here have converged, this equation can be solved for the next highest frequency, given the criterion for the frequency variance at the next highest frequency:

$$\text{Below 1 GHz,}\quad \sigma_{\hat{\phi}} = \frac{1 \text{ cycle}}{4*\text{Integration Time}}$$

After phase and frequency measurements are being made at frequencies above 1 GHz, two criteria have to be met. In addition to the frequency relation, Σ_k yields an analogous phase variance equation and criterion:

$$\sigma^2_{\hat{\phi}} = \sigma^2_{\hat{A}} f^2 + 2\,\sigma_{\hat{A}\hat{B}} + \sigma^2_{\hat{B}} f^{-2} \qquad (47)$$

$$\text{Above 1 GHz,}\quad \sigma_{\hat{\phi}} = 0.1 \text{ cycles (to prevent cycle-slip error)}$$

When predicting new frequencies above 1 GHz, both the phase and frequency predictions are made, and the lower frequency prediction is used. The measurement matrix (H_k) and the measurement covariance matrix (R_k) are enlarged to accommodate the additional phase and frequency measurements at the new transmitter frequency allocation.

In addition to these measurement criteria, the system designer can decide on other frequency allocations based on existing international frequency allocations. He still must meet the measurement criteria: that is, in order for the signal at the next highest frequency to

be tracked, the measurements of the signals at all lower frequencies must meet the two conditions shown above.

5. Results

The various factors determining the required transmitter power for unaided acquisition and aided tracking are shown below, in addition to the total required transmitter power as a function of frequency. Note how the dependence of acquisition bandwidth upon frequency dominates the power requirements at lower frequencies. Once the signal is acquired at the lowest frequency, however, one can take advantage of the decrease in ionospheric phase shifting as frequency increases. This decrease results in a slight drop in the power needed for the frequencies to be tracked, until atmospheric attenuation and vacuum path losses begin to dominate.

The fact that at frequencies under 9 GHz the required power for aided tracking is less than 1 w is encouraging. For a transmitter operating at a 1% duty cycle, broadcasting at 10 frequencies between 0.1 - 9 GHz, the average power required is 0.1 w. If one wanted to make studies of the water vapor content of the atmosphere, one could add on additional frequencies near the water vapor resonance (with the additional penalty in power required).

The calculated powers required for unaided acquisition and aided tracking reflect the contributions of many assumptions. One could transmit at less power than those dictated by Figure 19 to achieve other goals. For instance, one could measure water vapor content at the water vapor resonance at 22.5 GHz without necessarily having to track signal phase or frequency.

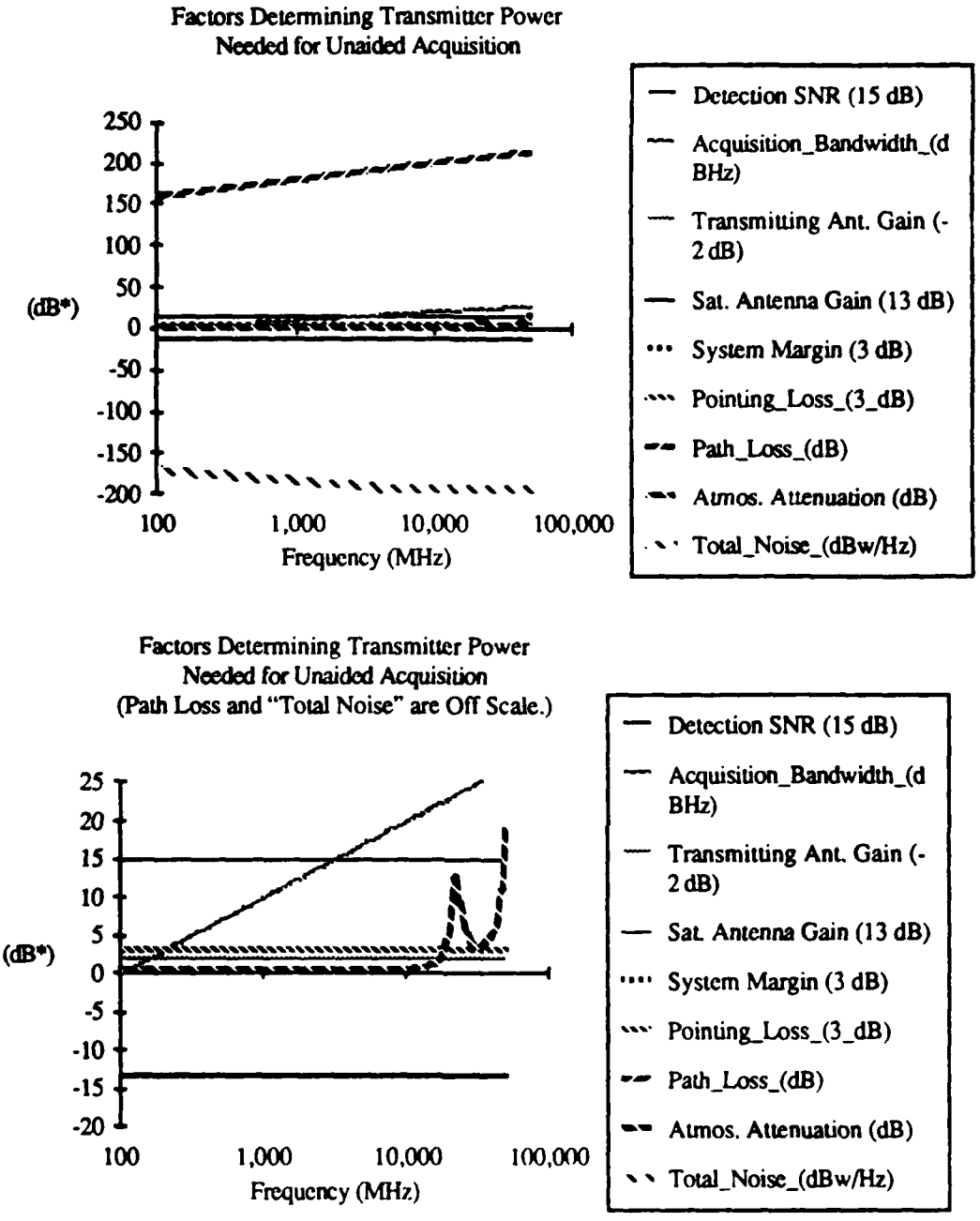

Figure 17. Factor Breakdown for Unaided Acquisition Power

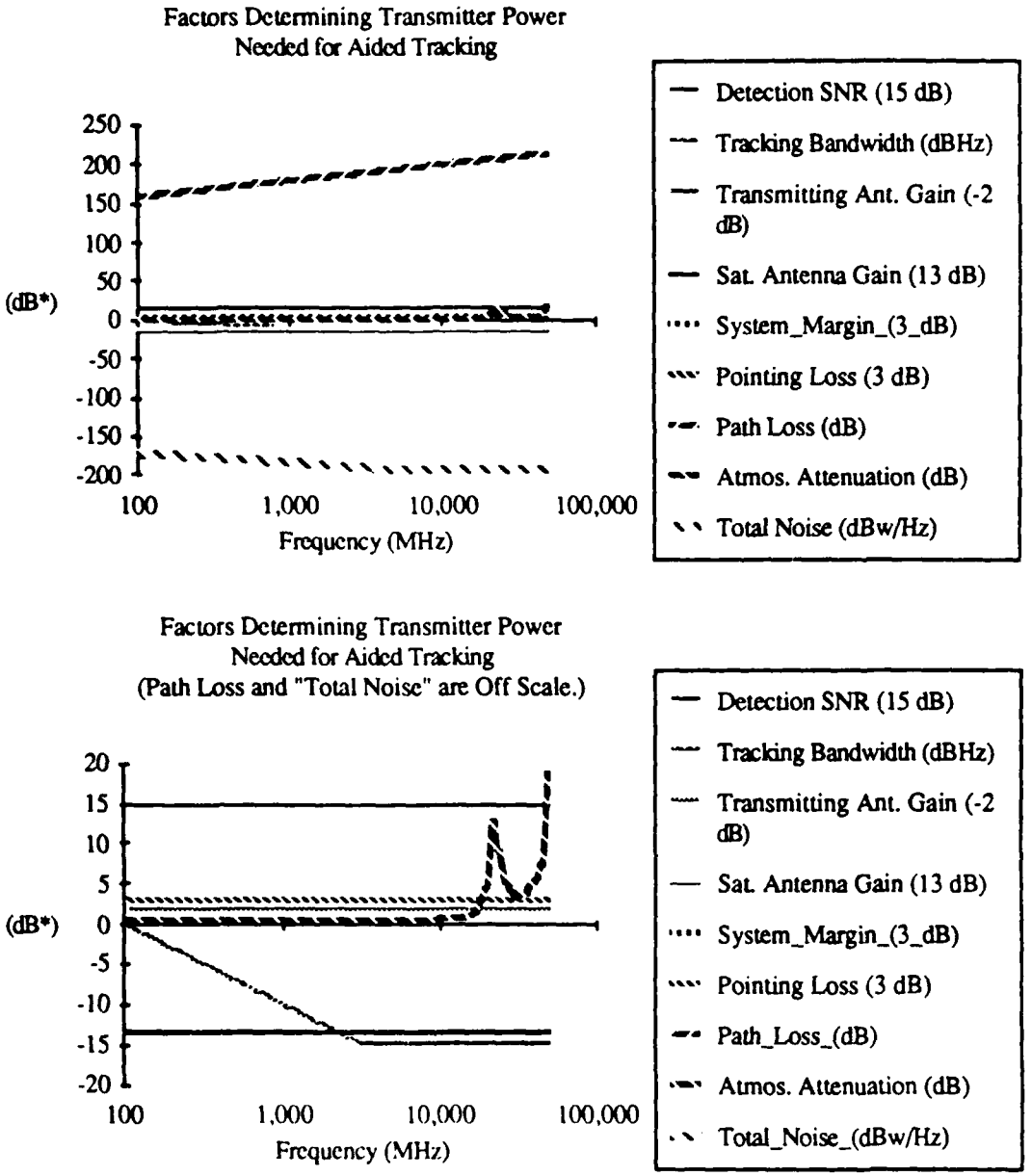

Figure 18. Factor Breakdown for Aided Tracking

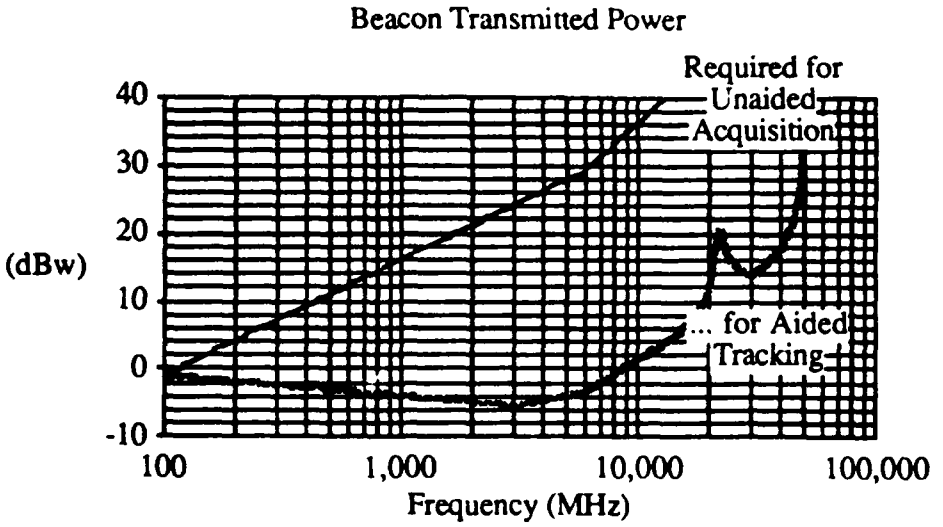

Figure 19. Uplink Power Budget

6. Conclusions

It is possible to design a relay satellite constellation which can accommodate low power (≤ 0.1 w) SAR and geodetic radio transmitters. By defining user positioning requirements one can perform an analysis of the radio spectrum to find candidate frequency allocations for a new system. There is a (growing) need to measure and control the effects of interfering man-made radio noise in space, as well as a need to study the possibilities of suitable frequency allocation sharing among different radio applications.

In addition to estimating the required uplink power, an algorithm has been shown which can be used to select transmitter frequencies which will maximize the positioning capability of the GeoBeacon transmitter. With simple models of the man-made electromagnetic noise environment in high earth orbits and of ionospheric behavior, a system designer can use a Kalman filter to make choices as to the most advantageous frequency allocations for this system. The Kalman filter can be used make frequency selections over a variety of levels of positioning accuracy; thus, this methodology for frequency selection can accommodate different user needs as well as man - made frequency allocation restrictions.

7. Recommendations

7.1. Improved Radio Noise and Interference Models

As demonstrated earlier, the piece of information with the greatest uncertainty is the noise temperature estimate from man-made noise (incidental and transmitter) from the Earth as seen from Earth orbit. This estimate would vary with altitude, frequency, weather, local time of day, and season. The ITU (International Telecommunications Union) has already foreseen this need and has issued recommendations for "propagation data required for the design of Earth-space telecommunication systems..." and "propagation data required for the evaluation of interference between stations in space and those on the surface of the Earth..."[1] The results of this study reinforce the need for these recommendations to be acted upon as soon as possible.

In addition, as more useful radio systems vie for a finite number of frequency allocations, it will become more important to have accurate measurements of the levels of interference which can be expected from other systems sharing the allocation. These measurements will need to be made at a variety of orbit altitudes in addition to the Earth's surface.

7.2. Improved Ionospheric Multipath Model

There is a need to understand the relations between ionospheric multipath scintillations and frequency. Once the expected phase change can be modeled as a function of frequency, the effects of measurements at lower frequencies in the Kalman filter can aid in the prediction of multipath effects at other frequencies.

---

[1]Recommendations 618 & 619, Recommendations and Reports of the CCIR, 1986.

7.3. AMSAT/OSCAR Experiment

Over the last 20 years, amateur radio operators have launched several OSCAR (Orbiting Satellite Carrying Amateur Radio) satellites into Earth orbit. Satellite activity in the United States has been organized by the Radio Amateur Satellite Corporation (AMSAT). Two AMSAT/OSCAR satellites, designated AO-10 and AO-13, are in highly elliptic inclined orbits (~4000 km by ~35000 km) which occasionally allows for continuous observation times on the order of several hours. These satellites are not repeaters, (linear transponders shift the signal from the uplink band to the downlink band), and the user is constrained to send a signal with a relatively narrow bandwidth of about 20 kHz. However, the satellites uplink frequencies (see table) could be used to perform crude baseline measurements with transmitters similar to those developed in this study.

Mode	Ground Station Transmit Band	Ground Station Receive Band
A	145.8 - 146.0 MHz	29.3-29.5 MHz
B	435.0 - 438.0 MHz	145.8 - 146.0 MHz
J	145.8 - 146.0 MHz	435.0 - 438.0 MHz
L	1260 - 1270 MHz	435.0 - 438.0 MHz

Table 4. Transponder Frequencies and Designations Used in the Amateur Satellite Service

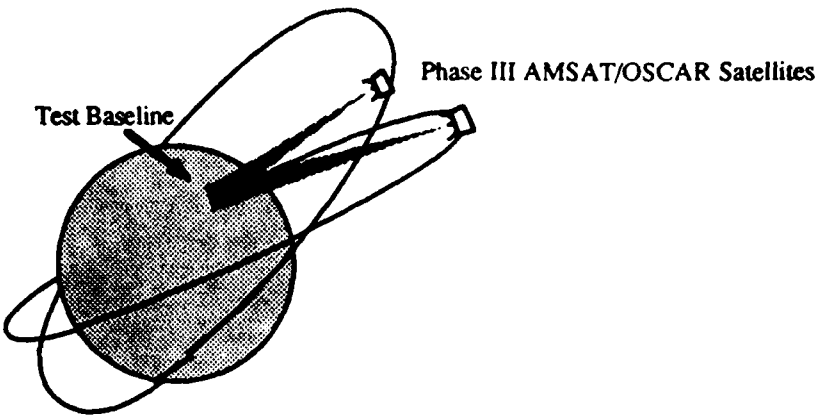

Figure 20. Possible AMSAT/OSCAR Baseline Measurement Experiment

8. Acknowledgements

The author completed this work while supported by a Minority Fellowship from the National Science Foundation (with tenureship covering the 1987-1990 academic years.) Work done with the Space Geodesy Group of the Center for Space Research was made possible by Air Force Contract F19628-86-K-0009 with the Air Force Geophysics Laboratory.

I want to thank several people for their help throughout the development of this work:

› Prof. Charles Counselman for his guidance and patience as I began my research in the CSR Space Geodesy Group. Through his insight, thoroughness, and encouragement during this study he has set an example I hope to pass on to others.

› Sergei Gourevitch for his welcomed advice throughout the study, particularly comments and help concerning Kalman filtering.

› Jayant Sharma for his availability for discussion of many topics in this study and for his enthusiastic support.

› Bill Irving for his constructive comments during the proofreading of this document.

9. Appendices

9.1. Calculation of Process Noise Covariances

$$E[x_1x_1] = \int_0^{\Delta t}\int_0^{\Delta t} g_1(u)g_1(v)\, E[w(u)w(v)]\, du\, dv \qquad (A.1)$$

$$= \int_0^{\Delta t}\int_0^{\Delta t} \frac{2\sigma_k^2}{\beta_k^3}(\beta_k u - 1 + e^{-\beta_k u})(\beta_k v - 1 + e^{-\beta_k v})\,\delta(u-v)\, du\, dv$$

$$= \frac{\sigma_k^2}{\beta_k^4}\left(\frac{2\beta_k^3\Delta t^3}{3} + 2\beta_k\Delta t - e^{-2\beta_k\Delta t} + 1 - 2\beta_k^2\Delta t^2 - 4\beta_k\Delta t\, e^{-\beta_k\Delta t}\right)$$

$$E[x_4x_4] = \frac{\sigma_i^2}{\beta_i^4}\left(\frac{2\beta_i^3\Delta t^3}{3} + 2\beta_i\Delta t - e^{-2\beta_i\Delta t} + 1 - 2\beta_i^2\Delta t^2 - 4\beta_i\Delta t\, e^{-\beta_i\Delta t}\right)$$

$$E[x_1x_2] = \int_0^{\Delta t}\int_0^{\Delta t} g_1(u)g_2(v)\, E[w(u)w(v)]\, du\, dv \qquad (A.2)$$

$$= \frac{2\sigma_k^2}{\beta_k^3}\left(\frac{1}{2} - \beta_k\Delta t + \frac{\beta_k^2\Delta t^2}{2} - e^{-\beta_k\Delta t} + \frac{e^{-2\beta_k\Delta t}}{2} + \beta_k\Delta t\, e^{-\beta_k\Delta t}\right)$$

$$E[x_4x_5] = \frac{2\sigma_i^2}{\beta_i^3}\left(\frac{1}{2} - \beta_i\Delta t + \frac{\beta_i^2\Delta t^2}{2} - e^{-\beta_i\Delta t} + \frac{e^{-2\beta_i\Delta t}}{2} + \beta_i\Delta t\, e^{-\beta_i\Delta t}\right)$$

$$E[x_1x_3] = \int_0^{\Delta t}\int_0^{\Delta t} g_1(u)g_3(v)\, E[w(u)w(v)]\, du\, dv \qquad (A.3)$$

$$= \frac{2\sigma_k^2}{\beta_k^2}\left(\frac{1}{2} - \frac{e^{-2\beta_k\Delta t}}{2} - \beta_k\Delta t\, e^{-\beta_k\Delta t}\right)$$

$$E[x_4x_6] = \frac{2\sigma_i^2}{\beta_i^2}\left(\frac{1}{2} - \frac{e^{-2\beta_i\Delta t}}{2} - \beta_i\Delta t\, e^{-\beta_i\Delta t}\right)$$

$$E[x_2x_2] = \int_0^{\Delta t}\int_0^{\Delta t} g_2(u)g_2(v)\, E[w(u)w(v)]\, du\, dv \qquad (A.4)$$

$$= \frac{2\sigma_k^2}{\beta_k^2}\left(-\frac{3}{2} + \beta_k\Delta t + 2e^{-\beta_k\Delta t} - \frac{e^{-2\beta_k\Delta t}}{2}\right)$$

$$E[x_5x_5] = \frac{2\sigma_i^2}{\beta_i^2}\left(-\frac{3}{2} + \beta_i\Delta t + 2e^{-\beta_i\Delta t} - \frac{e^{-2\beta_i\Delta t}}{2}\right)$$

$$E[x_2x_3] = \int_0^{\Delta t}\int_0^{\Delta t} g_2(u)g_3(v)\, E[w(u)w(v)]\, du\, dv \qquad (A.5)$$

$$= \frac{\sigma_k^2}{\beta_k}\left(1 - 2e^{-\beta_k\Delta t} + e^{-2\beta_k\Delta t}\right)$$

$$E[x_5x_6] = \frac{\sigma_i^2}{\beta_i}\left(1 - 2e^{-\beta_i\Delta t} + e^{-2\beta_i\Delta t}\right)$$

$$E[x_3x_3] = \int_0^{\Delta t}\int_0^{\Delta t} g_3(u)g_3(v)\, E[w(u)w(v)]\, du\, dv \qquad (A.6)$$

$$= \sigma_k^2\left(1 - e^{-2\beta_k\Delta t}\right)$$

$$E[x_6x_6] = \sigma_i^2\left(1 - e^{-2\beta_i\Delta t}\right)$$

9.2. Square Root Formulation of Discrete Kalman Filter

In this work, the discrete Kalman Filter equations (as shown in the frequency selection section) are used to propagate the state error covariance matrix from one observation time to the next. When implementing this algorithm on a computer, however, numerical roundoff errors can show up as negative diagonal terms in P_k, forcing the matrix to lose its positive definiteness. The problem occurs when the numerical range of values of P_k span over several orders of magnitude.

One technique used to solve this problem is to increase the process errors in Q_k. Another remedy, which does not require any model changes, is to propagate the matrix square root formulation of P_k, hereafter referred to as W_k. This cuts in half the logarithmic numerical range of the propagated values, diminishing the effect of roundoff error.

The relation between P_k and W_k is defined by the relationship

$$W_k W_k^T = P_k = \sum_{i=1}^{n} w_i w_i^T \qquad (A.7)$$

where

w_i = i^{th} column vector of the matrix W

n = the number of columns of W, which will be defined as the dimension of P_k .

With this definition, if P_k is positive definite, the column vectors w_k are linearly independent. It is generally desirable to force the column vectors of W_k to be linearly independent. Then when P_k is positive semi-definite some column vector or vectors will be null. The rank of P_k is equal to the number of non-zero column vectors of W_k in this formulation.

The discrete Kalman filter algorithm remains the same, except for the fact that we are propagating the square root formulation of P_k instead of P_k itself. This will require three modifications to the computer implementation:

i) Calculate W_0, given P_0.

ii) Extrapolating W_k forward in time (Calculate $W_k(-)$, given $W_{k-1}(+)$, instead of calculating $P_k(-)$ from $P_{k-1}(+)$).

iii) Incorporating measurements into W_k (Calculate $W_k(+)$, given $W_k(-)$, instead of calculating $P_k(+)$ from $P_k(-)$).

To make the modification required in (i), one must look at the initial state covariance matrix P_0. The initial error estimates are based on *a priori* knowledge of transmitter position and kinematics, as well as ionospheric behavior. Since these estimates are all independent, P_o is a diagonal matrix. Consequently, W_0 is a diagonal matrix with standard deviations of the initial estimates as the entries.

$$P_0 = \begin{bmatrix} \sigma^2_{\hat{a}} & & \\ & (6 \times 6) & \\ & & \sigma^2_{\dot{\hat{\beta}}} \end{bmatrix} \qquad W_0 = \begin{bmatrix} \sigma_{\hat{a}} & & \\ & (6 \times 6) & \\ & & \sigma_{\dot{\hat{\beta}}} \end{bmatrix}$$

In order to propagate W_k as required in (ii), it is assumed that the process noise covariance matrix Q_k is available in factored form similar to P_k:

$$R_k = \sum_{i=1}^{j} s_i s_i^T = S_k S_k^T \qquad (A.8)$$

where

s_i = linearly independent vectors

j = number of random forcing functions

For this case, R_k has two 3 by 3 block matrices along its diagonal. Although there are in infinite number of possibilities for S_k, there is only one where the s_i are mutually orthogonal. This is found by solving for the eigenvalues and eigenvectors of R_k. Since R_k is real and symmetric it can be decomposed into the form shown below.[1] In addition, since R_k is positive definite, its eigenvalues will be real.

$$R_k = S_k S_k^T = (V \Lambda^{1/2})(\Lambda^{1/2} V^T) \qquad (A.9)$$

[1]Strang, Introduction to Applied Mathematics, p. 61.

$$= \begin{bmatrix} \underline{v}_1 & \underline{v}_2 & \underline{v}_3 & \underline{v}_4 & \underline{v}_5 & \underline{v}_6 \end{bmatrix} \begin{bmatrix} \lambda_1^{1/2} & & & & & \\ & \lambda_2^{1/2} & & & & \\ & & \lambda_3^{1/2} & & & \\ & & & \lambda_4^{1/2} & & \\ & & & & \lambda_5^{1/2} & \\ & & & & & \lambda_6^{1/2} \end{bmatrix}$$

$$\begin{bmatrix} \lambda_1^{1/2} & & & & & \\ & \lambda_2^{1/2} & & & & \\ & & \lambda_3^{1/2} & & & \\ & & & \lambda_4^{1/2} & & \\ & & & & \lambda_5^{1/2} & \\ & & & & & \lambda_6^{1/2} \end{bmatrix} \begin{bmatrix} \underline{v}_1^T \\ \underline{v}_2^T \\ \underline{v}_3^T \\ \underline{v}_4^T \\ \underline{v}_5^T \\ \underline{v}_6^T \end{bmatrix}$$

where

$\lambda_i = i^{th}$ eigenvalue

$\underline{v}_i = i^{th}$ eigenvector ($\| \underline{v}_i \| = 1$)

The block submatrices of R_k simplify this calculation, since the eigenvectors must now have the form shown below. In addition, since this matrix is positive definite, all of its eigenvalues must be positive.

$$R_k = \begin{bmatrix} * & * & * & 0 & 0 & 0 \\ * & * & * & 0 & 0 & 0 \\ * & * & * & 0 & 0 & 0 \\ 0 & 0 & 0 & * & * & * \\ 0 & 0 & 0 & * & * & * \\ 0 & 0 & 0 & * & * & * \end{bmatrix}$$ yields 3 eigenvectors of the forms $\begin{bmatrix} * \\ * \\ * \\ 0 \\ 0 \\ 0 \end{bmatrix}$ and $\begin{bmatrix} 0 \\ 0 \\ 0 \\ * \\ * \\ * \end{bmatrix}$

With S_k defined, the extrapolation proceeds as follows:

a) Let $A_1 = [\Phi W_{k-1}(+) \mid S_k]$ (A.10)

Iterate steps (b) through (e) for j=1,..n where $v_j(l) = \begin{cases} 0 & l \neq j \\ 1 & l = j \end{cases}$

b) $\overline{w}_j = A_j A_j^T v_j$ (A.11)

c) $M_j = I - \dfrac{\overline{w}_j v_j^T}{\overline{w}_j(j)}$ (A.12)

d) $A_{j+1} = M_j A_j$ (A.13)

e) $w_j = \dfrac{\overline{w}_j}{\sqrt{\{\overline{w}_j\}}}$ (A.14)

The w_j calculated in (e) are the columns of the extrapolated $W_k(+)$. Finally, for the measurement update, as specified in (iii), the measurements are processed one at a time:

For each measurement (2 * (# of frequencies) iterations),

a) $v = W_k^T(-)H_k^T$ (A.15)

b) $u = W_k(-)v$ (A.16)

c) $a = (v^T v + Q_k)\left(1 + \sqrt{\dfrac{Q_k}{v^T v + Q_k}}\right)$ (A.17)

d) update: $W_k(+) = W_k(-) - \dfrac{uv^T}{a}$ (A.18)

Since this sequence is iterated for each measurement, there is no need to invert any matrices as in the standard discrete Kalman filter. This change reduces computational effort as the number of frequencies being tracked increases.

10. References

Agrawal, Brij N., Design of Geosynchronous Spacecraft, Prentice-Hall, Inc., Englewood Cliffs, NJ, 1986.

Battin, Richard H., An Introduction to the Mathematics and Methods of Astrodynamics, AIAA Education Series, 1987.

Bierman, Gerald J., Factorization Methods for Discrete Sequential Estimation, Academic Press, 1977.

CCIR, Report 396-5, Annex VI, "Maintenance Telemetering, Tracking, and Telecommand for Developmental and Operational Satellites," in Volume II, Recommendations and Reports of the CCIR, 1986, pp. 158 - 170, International Telecommunications Union, Geneva, 1986.

Counselman, III, Charles C. and Gourevitch, Sergei A., "Miniature Interferometer Terminals for Earth Surveying: Ambiguity and Multipath with Global Positioning System," IEEE Transactions on Geoscience and Remote Sensing, Vol. GE-19, No.4, October 1981.

Counselman, III, Charles C., Method and System for Determining Position Using Signals from Satellites, United States Patent #4,667,203, May 19, 1987.

Crane, R.K., "An Algorithm to Retrieve Water Vapor Information from Satellite Measurements," NEPRF Tech. Rept. 7-76 (ERT) Final Report, Project No. 1423, Environmental Research and Technology, Inc., November 1976.

Davidoff, Martin R., The Satellite Experimenter's Handbook, American Radio Relay League, Newington, CT, 1985.

Gelb, Arthur, Applied Optimal Estimation, MIT Press, Cambridge, MA, 1974.

Herman, J. R., "The Radio Noise Environment in Near Space: A Review," Proc. IEEE International Symposium on Electromagnetic Compatibility, June 20 - 22, 1978.

Herring, Thomas A., notes from a presentation given at MIT, October 26, 1988.

Ippolito Jr., Louis J., Radiowave Propagation in Satellite Communications, Van Nostrand Reinhold Company, New York, 1986.

ITU Radio Regulations, International Telecommunication Union, Geneva, 1982.

Jordan, Thomas H. and Minster, J. Bernard, "Measuring Crustal Deformation in the American West," Scientific American, August, 1988. pp. 48 - 58.

King, R. W., Masters, E. G., Rizos, C., Stolz, A., and Collins, J., Surveying With GPS, Monograph 9, School of Surveying, The University of New South Wales, Kensington, N.S.W. Australia, 1985.

Schmidt, S.F., "Computational Techniques in Kalman Filtering," Theory and Applications of Kalman Filtering, Advisory Group for Aerospace Research and Development, AGARDograph 139, (AD 704 306), Feb. 1970.

Skomal, Edward N., "Analysis of Spaceborne VHF Incidental Noise Over the Western Hemisphere," IEEE Transactions on Electromagnetic Compatibility, Vol. EMS-25, No. 3, August 1983, pp. 321-328.

Skomal, Edward N. and Smith, Albert A., Measuring the Radio Frequency Environment, Van Nostrand Reinhold Company, New York, 1985.

Smith, Ernest K. and Njoku, Eni G., "The Microwave Noise Environment at a Geostationary Satellite Caused by the Brightness of the Earth," Symposium Record: IEEE 1985 International Symposium on Electromagnetic Compatibility, August 20-22, 1985.

Spilker Jr., J.J., "GPS Signal Structure and Performance Characteristics," Global Positioning System, Navigation, Journal of the Institute of Navigation, Vol.25, No. 2, 1978.

Strang, Gilbert, Introduction to Applied Mathematics, Wellesley - Cambridge Press, Wellesley, MA, 1986.

van Graas, Frank, "Sole Means Navigation Through Hybrid Loran-C and GPS," Navigation: Journal of the Institute of Navigation, Vol. 35, No. 2, Summer 1988.

Wells, David, Guide to GPS Positioning, Canadian GPS Associates, Fredericton, N.B Canada, 1986.

Wenzel, Robert J., "Omega Navigation System - A Status Report," Navigation: Journal of the Institute of Navigation, Vol. 35, No. 3, Fall 1988.